Managing resilience and viability of supranational supply chains under epidemic control scenarios

Managing resilience and viability of supranational supply chains under epidemic control scenarios.

—— Author's Version ——

Jan B. Broekaert[a,*], Faizal Hafiz[a], Raja Jayaraman[b], Davide La Torre[a]

[a]*SKEMA Business School, Université Côte d'Azur, Sophia Antipolis, France*
[b]*Department of Industrial Engineering,*
New Mexico State University, Las Cruces, NM, United States

Abstract

A comprehensive model is presented to evaluate the *resilience* and *viability* of supranational supply chains under various epidemic control scenarios. The model integrates a multiplex network of socially connected individuals subjected to a probabilistic SEIRSD epidemic, as well as production configurations monitored for performance capacity. The epidemic evolution within this system depends on four primary cost factors: deployed control strategy, health policy implementation, the value of human life, and economic productivity loss due to the epidemic. These costs are adjusted for GDP differences between countries in the network and are influenced by factors such as the duration and severity of confinement, vaccination efficacy, and healthcare capacity. A Nash equilibrium analysis of SEIRSD load-based costs is employed to identify optimal control strategies. Time To Recovery (TTR) and Longitudinal Service Level (LSL) are used as metrics for assessing the resilience and viability of supply chains. The convergences and conflicts of control strategies are evaluated using TTR and LSL, providing insights into the impact of public health measures on supply chain performance. This methodology offers a framework for policymakers and supply chain managers to make informed decisions during prolonged epidemic conditions. Numerical simulations illustrate the conditions for convergence and conflict between epidemic control policies and supply chain objectives, highlighting the need for dynamic policy adjustments to ensure supply chain resilience and viability.

*Corresponding author

Email addresses: jan.broekaert@skema.edu (Jan B. Broekaert), faizal.hafiz@skema.edu (Faizal Hafiz), rjayaram@nmsu.edu (Raja Jayaraman), davide.latorre@skema.edu (Davide La Torre)

1. Introduction

When a global calamity strikes, various governmental mitigation strategies are implemented worldwide, adding further profound impact on industry and business processes. The most recent case in point, the COVID-19 pandemic, prompted diverse policies from governments and health authorities globally, resulting in significant local and global economic downturn (Jackson et al., 2021; Ajmal et al., 2021; Lofvers, 2020). The manufacturing, processing, and shipping sectors along supply chains experienced unpredictable disruptions to their performance capacities, inventory issues, stockouts, and price surges in first materials and commodities (Lofvers, 2020; Hille, 2021; Ardolino et al., 2022). Public policymakers have deployed several control strategies based on epidemic dynamics modeling to mitigate the impacts (Bertozzi et al., 2020; Godio et al., 2020; Reicher and Stott, 2020; Boucekkine et al., 2021; MacIntyre et al., 2021; Xu et al., 2021; Yang, 2021; Amir and Boucekkine, 2022; Dobson et al., 2023).

These control strategies, which involve different forms of social distancing to limit transmission and vaccination policies to boost immunity, aim to minimize the epidemic burden—quantifiable in both economic and human-life terms—within their respective territory. However, these measures interrupt normal industrial and business operations. The performance of supply chains and epidemics converge in their core property of diverse geographic industrial and business implantation, and interdependence of labor actors. This interdependence is crucial in a social population where it is also the enabling factor of disease propagation. In supply chain networks the diversified localization of service and production and their interdependence is a contingent business structure derived from planning, cost optimization, and product complexity requiring the assembling and dispatching of first and derived materials. The interconnection in these networks entails that a disruption in one location can quickly affect operation in others, similar to how a virus spreads through a population. The common underlying feature of interdependence between the same population of individuals allows –possibly up to a scale factor– their functioning as common nodes in two layers on one network. The simultaneous implementation of different mitigating strategies by international policymakers has a complex impact on supranational supply networks. Our previous work (Broekaert et al., 2024b) aimed to predict how international supply chains could be reconfigured following policymakers' mitigation strategies. First, a game-theoretic ap-

proach was employed in our model to derive Nash equilibrium profiles from diverging control strategies by connected countries with different GDPs, based on optimal **E**pidemic **C**ontrol **C**osts (ECC).[1] Then, from a matrix of throughput **L**oss and **M**igration **C**osts (LMC) for divergent policies, a method was derived to assess potential supply chain reconfigurations.

In our current study, we analyze how diverse control policies converge or conflict with supply chain-centered objectives. Our method starts by deriving the Epidemic Control Cost (ECC) matrix for divergent mitigation policies of two international policymakers and determining the optimal Nash strategy profile. In contrast, alternative optimal Nash strategy profiles are determined for two core supply chain metrics. Comparing these supply chain metric-based Nash profiles with the ECC-based Nash profiles reveals conditions for convergence and conflict of mitigation strategies. Our original contribution presents managers and policymakers with a framework to comprehend how public policies affect and should be informed by supply chain performance.

In an interconnected contact network spanning different countries, and where epidemic control policies mutually influence outcomes, the *resilience* and *viability* of international supply chains are consequently affected (Ivanov and Dolgui, 2020). To formally assess these supply chain characteristics, we propose appropriate metrics: the resilience of supply chains, monitored through their **T**ime **T**o **R**ecovery (TTR), and the viability of supply chains, quantified using their **L**ongitudinal **S**ervice **L**evel (LSL).[2] The Time To Recovery measures the time a supply chain –or a defined portion of it– takes to recover its normal operational performance after a disruption, with a shorter TTR indicating higher resilience. The Longitudinal Service Level, based on the practical Service Level –the percentage of customer demand met without delay from the available inventory– monitors the robustness in meeting a series of process-impacting shocks while keeping an effective service. The Longitudinal SL impacts customer satisfaction and market competitiveness by demonstrating reliability in meeting customer demand over time. Emphasizing the longitudinal aspect using LSL then assesses the long-term viability of supply chains under repeated disruptions.

[1] The ECC in our model is formally defined in Eq.(12).

[2] Both metrics TTR and LSL are formally defined in Eqs. (2) and (7) repectively. See also e.g. Ruel et al. (2024) and Falasca and Zobel (2008) for alternative uses.

Our study details the convergences and conflicts in control policies for a configuration involving two regions, capturing the basic dynamics of large-scale contact networks. Under disruptions, supply chain managers seek a control strategy profile that *minimizes* the TTR and *maximizes* the LSL of their supply chains. Policymakers, referred to as 'players' in a strategic game, determine the optimal control policy for each epidemic wave by considering the Nash equilibrium of the ECC. The cost-based Nash equilibrium dictates the isolation measures and control profiles for policymakers, focusing on public cost optimization, which may conflict with supply chain managers' concerns.

This Nash strategic profile impacts both TTR and LSL and its monitoring hence allowing the assessment of supply chain *resilience* and *viability*. Besides the Nash equilibrium of the ECC, the policymakers can identify the Nash equilibria for TTR and LSL to inform their policy, or alternatively, they can directly identify an optimal strategy for a weighted scalarized goal encompassing all three. Hence, continuous monitoring of TTR and LSL can enable dynamic policy adjustments in response to changing epidemic conditions, ensuring that supply chains remain resilient and viable over time.

The remainder of the paper is organized as follows. Section 2 reviews significant literature on supply chain behavior under disruptions, particularly epidemiological models on social-contact networks. Section 3 covers the concepts of the multiplex model with a production layer to model supply chain activity levels, providing TTR and LSL metrics informing supply chain managers, and an epidemiological layer informing the ECC for policymakers. Here the specific epidemic model is detailed, obtaining its acronym from the defining population segments or characteristics related to the stages of the disease; ***S**usceptible*, ***E**xposed*, ***I**nfectious*, ***R**ecovered* and ***D**ead*, resulting in the 'SEIRSD' model - now with a second 'S', due to including the process of waning immunity.[3] Section 4 explains the methods and formal dynamics that underlie the encompassing supply chain & epidemic system, while the exact mathematical formalism is relayed in Appendix A and Appendix B. Section 5 presents numerical outcomes for health control strategies from Nash equilibria of ECC, TTR, and LSL, on a simulated network epidemic, along with an analysis of conditions for conflicts and

[3]The shorthand SEIRD is used to denote the *separate* characteristics.

convergences in optimal control policies. Here based on our model metrics, the framework for policymakers and supply chain managers emerges to make informed decisions during prolonged epidemic conditions, ensuring the resilience and viability of supply chains. Finally, Section 6 concludes by emphasizing our key insights into evaluating the resilience and viability of supply chains under control policies, as well as outlining the next steps for future research.

2. Literature overview

This section briefly reviews the literature on epidemic networks and their impact on supply chain resilience and viability, as well as game-theoretic approaches to managing these interdependencies.

Supply Chain Resilience and Viability. The concepts of resilience and viability in supply chains have been extensively studied. Juan et al. (2022) model the relationships among five components of supply chain resilience—visibility, velocity, flexibility, robustness, and collaboration—and their impact on performance during disruptions, identifying collaboration as a key driver. Chowdhury and Quaddus (2017) develop a resilience framework based on dynamic capability theory, highlighting proactive and reactive capabilities and supply chain design quality. Ivanov (2024b) used a hybrid bibliometric and expert approach to observe a shift from preparedness to recovery and proactive adaptation. Their related study (Ivanov, 2024a), on the resilience of supply chains, implements an ontology akin to the immune system with characteristics of preparedness and recovery, respectively translated by innate and adaptive immunities in a living system. Resilience as a system-wide quality over multiple industries is explored by Gruchmann et al. (2024), their online surveysshows the main factors of proactive preparedness via anticipation and reactive responsiveness via agility. In Echefaj et al. (2024b), the relationships between adaptation capabilities and practices ensuring operational continuity in supply chains were empirically tested and positively supported using responses from 252 organizations.

The work of Rozhkov et al. (2022), focuses on the adaptivity of operational decisions on preparedness and recovery in various network ontologies, pre and peri-pandemic: in particular the impact of anticipatory inventory pre-positioning and en route adaptation of production-ordering policy. The COVID-19 pandemic has generated significant research on sup-

ply chain disruptions. Decision-support models using epidemic dynamics have been proposed (Paul et al., 2021; Ouardighi et al., 2022), and the ripple effect in supply chains has been modeled extensively (Borgatti and Halgin, 2011; Mishra et al., 2019; Kinra et al., 2020; Li and Zobel, 2020; Park et al., 2021; Llaguno et al., 2021; Ivanov et al., 2020; Ivanov, 2020; Yu and Aviso, 2020; Choi, 2021; Sawik, 2022; Scarpin et al., 2022; Brusset et al., 2022, 2023), e.g. with the effect of long-term disruptions qualitatively analyzed using secondary data from automotive and electronics industries by Kravchenko et al. (2024).

The authors Ruel et al. (2024) propose a resource-based scale for supply chain viability using five factors 'structure and mechanisms', 'system development', and supply chain 'redesign', 'feedback', and 'process', and show its relation to supply chain performance under severe disruptions by providing a respondent-based nomological validation. Ivanov (2024c) explore adaptation- vs stability-based resilience, showing return to normal states compared to proactive adaptation are complementing quantitative and qualitative oriented protective approaches.

Network Models describe the dynamic interaction of diverse agents, ranging from individuals to firms, cities, or countries, in the movement of goods, wealth, people, labor, or health (Keeling and Eames, 2005; Newman, 2018). For example, intertwined supply chain networks were studied by Echefaj et al. (2024a) for their effects on sourcing and recovery strategies and, showing its recovery processes deviate from conventional patterns. Recent studies have focused on individual-based ontologies and the architecture of contact graphs to implement mitigating factors and assess impacts on labor productivity (Das et al., 2023). Multiplex network approaches incorporate additional features, such as an information layer for disease awareness diffusion (Fan et al., 2022) and competing opinions over social-contact networks (Peng et al., 2021). These models enable a detailed assessment of the impact on supply chains. An optimized network-of-networks mechanism for cross-industry adaptation during crises was proposed for, and gains examined from, collaborative crisis preparedness by Dolgui et al. (2024).

Control Policies and Epidemic Costs. Epidemic models have been developed to assess the mitigating effects of control policies. Eryarsoy et al. (2023) solve a compartmental SEIRD-model with time-dependent infection rates and government stringency indices. Chen et al. (2023) build a SIRD-model linking social distancing policies to financial market stability.

The overall epidemic cost has been modeled by several studies (Charp-

entier et al., 2020; Reddy et al., 2021; Gros et al., 2021; Gollier, 2021; Plazas et al., 2021). Long-term effects on wealth redistribution are considered by Boucekkine and Laffargue (2010), while Huberts and Thijssen (2023) develop a non-pharmaceutical mitigation model to minimize social epidemic costs.

Game-Theoretic Approaches. The interconnection of populations on a global contact network means local control policies impact epidemic outcomes beyond their jurisdictions. The COVID-19 pandemic highlighted the need for regulatory flexibility and political enabling for effective supply chain management (Farahani et al., 2023). da Fonseca et al. (2023) demonstrate the importance of firm-to-firm technology transfer for large-scale vaccine production. Game-theoretic models have been used to study competitive acquisition of medical supplies (Salarpour and Nagurney, 2021) and the optimal allocation of resources (Nagurney et al., 2016; Nagurney, 2021a,b). These models highlight the co-determinacy of epidemic outcomes due to interlinked populations and the necessity for collaborative strategies.

3. The supply chain and epidemic network model

Building on previous studies involving our epidemic model (Broekaert et al., 2022, 2024c,a,b), we adopt a multiplex graph ontology that integrates a supply chain production layer with the population's social contact layer under a SEIRSD epidemic dynamic. The model incorporates distinct epidemic *control strategies* deployed by two interconnected population groups on the contact graph –which can typically be referred to as 'regions' or 'countries'. These controls induce changes in the graph topology and population characteristics over time, resulting in a temporally heterogeneous epidemic graph model, e.g. Fig. 1. The new features in our current model facilitate the description of supply chain *viability* and *resilience*.

Basically, an individual-based network model spans a *graph* by linking all human individuals -or nodes - that experience a 'person-person' interaction that can cause the contagious disease to spread. These shared-location-based networks have a different topology in comparison to 'social networks' based on social media connections (Barrett et al., 2009; Prasse et al., 2021).

Our models utilize an individual-based ontology and a probabilistic approach to provide the necessary variables for a quantitative analysis of *resilience* and *viability*. Each individual's probabilities of carrying disease characteristics in the supply chain form the basis for the expressions of Time

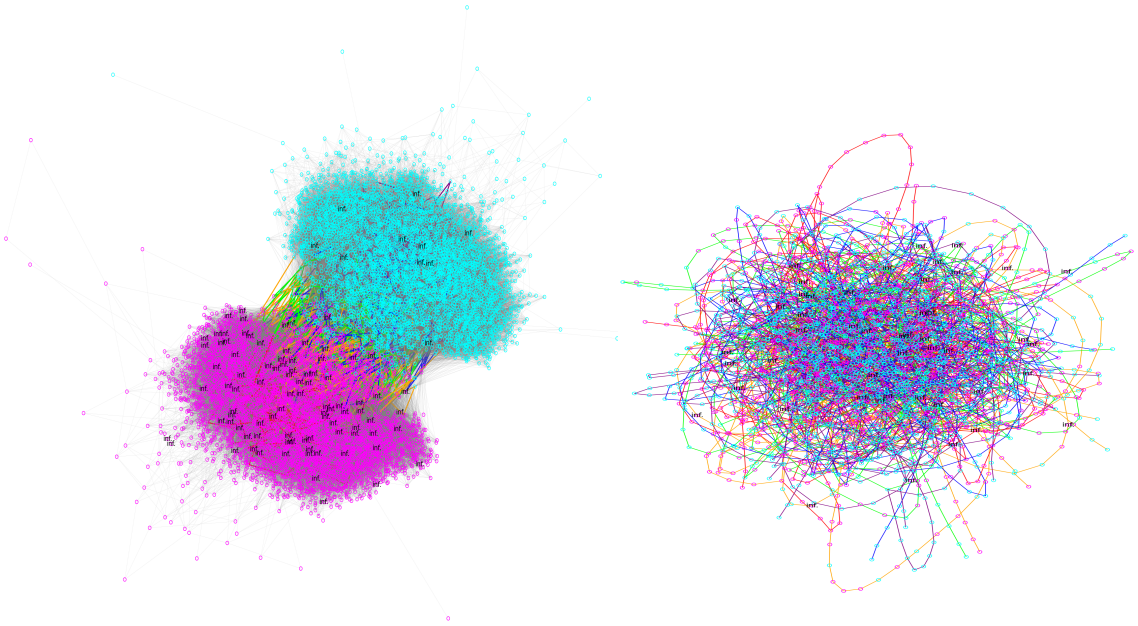

Figure 1: A simulated multiplex network (left) with supply chains spanning two distinct but interconnected regions (magenta vs. cyan) within a designed social contact graph $\mathscr{G}(V_{\mathscr{G}}, E_{\mathscr{G}})$ with $N = 10^4$ nodes, constructed using an optimized adjacency algorithm. For clarity, the Ifs_{01} isolation is depicted, which causes the full separation of the two regions. In each simulation of a controlled epidemic, ten random supply chains are tested for each of the varying spreads between the regions. The supply chain layer (right) groups the node sets that are active within and between the regions. The color coding for the spread values over the two regions is as follows:$\{0 : \text{`}purple\text{'}, .25 : \text{`}blue\text{'}, .5 : \text{`}lime\text{'}, .75 : \text{`}orange\text{'}, 1 : \text{`}red\text{'}\}$. Note that a spread value of 0 represents a supply chain entirely within group_1, while a spread value of 1 represents a supply chain entirely within group_0. Intermediate spread values indicate a mix of inter-group supply chains. The initially infected nodes are labeled 'inf.' and, mainly occur in group_0. (init_infected_wave1=100, spread_infect=.9)

To Recovery (TTR) and Longitudinal Service Level (LSL). The TTR and LSL metrics serve as proxy expressions for the concepts of *resilience* and *viability* in supply chains, respectively. Various other metrics were proposed to cover the inherent adaptability of the supply chain, particularly due to internal factors associated with mass customization manufacturers. Among these, the Time-to-Adapt (TTA) metric was introduced, which measures the time period from the onset of disruptions until actions are taken by the manufacturer to mitigate the effects (Mosayebi et al., 2024).

In the SEIRD epidemic model, each individual is assigned probabilities for possesing attrited characteristics (Exposed, Infectious, and Dead) and healthy characteristics (Susceptible and Recovered). These epidemic charac-

teristics change for each individual over time and depend on their contacts and epidemic control measures, as illustrated in Fig. 2. Their values influence an individual's health and, consequently, the effective performance capacity of the supply chains in which they operate, as expressed by the SEIRD-based definitions of TTR and LSL.

Time To Recovery - Using SEIRD Probabilities for TTR. In the SEIRSD model, the recovery process is captured by the transition from the Infected (I) state to the Recovered (R) state. However, also the Susceptible (S) state qualifies an individual to participate in the **S**upply **C**hain (SC) activities. For each node k in the supply chain subset V_{SC}, the total probability of being in a performing state at time t is $p_{R_k}(t) + p_{S_k}(t)$. This metric is hence the core parameter to assess the well-being of each individual k and their capability to perform labor. In the worst of the disease, this metric could drop low to 0 while someone uninfected or vaccinated will remain close to 1. It is hence crucial to know this metric for all people performing labor in a given supply chain. The expected Time To Recovery for individual k can be derived from the projected recovery probability over time, according to Eq. (B.1) which governs the epidemic spreading in a network. It suffices to extract the moment in time when this individual has regained sufficient capacity to regain labor activity. The TTR for the entire supply chain (SC), with node subset V_{SC}, can be defined as the average time at which its nodes have transitioned to a sufficiently performant state (S and R). *After* having evolved past the maximum peak value of the Exposed and Infected components in time, lowered probabilities in these components may not be indicative of disease incapacitation anymore. Accordingly, to encompass the variable degrees of *operational* recovery, a *performance threshold* value on the activity level $p_{R_k} + p_{S_k}$ is set above which an individual is considered to be capable of effectively performing labor again.[4]

Formally, for each node k in V_{SC}, the expected recovery time TTR_k can be estimated as the time when $p_{R_k}(t) + p_{S_k}(t)$ again reaches a threshold value perf_thresh, *after having passed its minimum activity level*:

$$\text{TTR}_k = \min\{t \mid p_{R_k}(t) + p_{S_k}(t) \geq \text{perf\_thresh and } t > t_{\min_k}\} \tag{1}$$

[4]The probabilistic node-states under the governing equations Eqs. (B.1) cannot, from a mathematical point of view, fully recover because the D-characteristic operates as a *sink* in the dynamics.

In real-world epidemics, practical considerations should decide the threshold value $\mathrm{perf\_thresh}$. The specific nature of the supply chain may require more stringent (e.g. medical, nursing, or elderly care) or permissive (agricultural, nautical, or industrial) thresholds. In the present simulation model with COVID-19 parametrization, the threshold is set to a demographic average, $\mathrm{perf\_thresh} = .7$, inciting labor re-activation under prolonged adverse conditions. The aggregated $\mathrm{TTR}_{V_{SC}}$ for the supply chain subset V_{SC} can be taken as the *average* of the node-level TTR_k, with $k \in V_{SC}$. Ultimately, the robust metric for assessing the supply chain's TTR is derived by averaging the $\mathrm{TTR}_{V_{SC}}$ for a large sample, N_{SC}, of supply chains – with the same typical regional spread – to obtain:

$$\mathrm{TTR} \;=\; \frac{1}{N_{SC}} \sum_{i=1}^{N_{SC}} \sum_{k \in V_{SC\,i}} \frac{\mathrm{TTR}_k}{|V_{SC_i}|} \tag{2}$$

which is essentially dependent on the epidemic wave (w), the spreading of the supply chain over the regions (*spread value*), and the **C**ontrol **S**trategy profile CS –listed in Eq.(10). The current definition for TTR, Eq. (2), is based on the underlying SEIRD model which expresses recovery and labor capacity from epidemic metrics. In real-world configurations, these epidemic metrics will instigate higher-level disruptions that are not reversible or suffer from substantial latency and which will prolong the effective TTR.

Service Level - Using SEIRD Probabilities for SL. The viability of a supply chain is evaluated by determining its Service Level (SL) within a longitudinal or multi-wave epidemic framework. In the proposed model, the service level of a supply chain is correlated with the potential for activity within the supply chain. Individuals performing in the supply chain, and with a high probability of infection will reduce its overall service level.

The activity probability p_{A_k} of a node is defined as the sum of the susceptibility probability and the recovered probability:

$$p_{A_k}(t) = p_{S_k}(t) + p_{R_k}(t), \tag{3}$$

as these are the characteristics that allow disease-unburdened labor. In the COVID-19-based SEIRSD model, only minor traces of Infected (I) and Exposed (E) states, along with a relatively small death probability (D), persist in the long term. Therefore, a minimum activity level during an

epidemic wave can be identified for each individual:

$$p_{A_k,\text{min}} = \min\{p_{A_k}(t)|t \in [0, T_w]\} \tag{4}$$

i.e., for each individual in the supply chain, the minimum activity over time $p_{A_k,\text{min}}$ is considered an indicator of potential activity failure in the given time window of the epidemic wave w. To capture the interdependence of activity within the supply chain with subset V_{SC}, the activity metric of the entire supply chain is calculated as the *harmonic* mean of the individual minimum activity levels of its nodes:

$$A_{V_{SC}} \quad = \quad l_{SC} \left(\sum_{k \in V_{SC}} (p_{A_{k,\text{min}}})^{-1} \right)^{-1} . \tag{5}$$

The harmonic mean is utilized because it emphasizes smaller values, ensuring that nodes with lower activity levels have a more significant impact on the overall metric. The robustness of the metric is practically assured by averaging the activity levels $A_{V_{SC}}$ of a number N_{SC} of supply chains with the same characteristic *spread value*:

$$\bar{A}_{V_{SC}} \quad = \quad \frac{1}{N_{SC}} \sum_{k=1}^{N_{SC}} A_{V_{SC}}. \tag{6}$$

This procedure avoids biased reporting of values based on the possibility of *atypical* random sampling of nodes –see Section 4. To track the effect of the control strategies (CS) on the supranational supply chains, the parameter *spread value* indicates how many segments of the supply chain depend on the health controls rolled out by each of the country's policymakers. To standardize its meaning the size of the supply chain node-set was fixed $V_{SC_i} = l_{SC}$ for all i, and the spread value is defined to express the fraction of the supply chain in country 0.

The longitudinal perspective of viability considers the repeated disruptions of three consecutive epidemic waves, each characterized by a distinct infectivity parameter(β) and, for which the *initial* SEIRD state is reset by combining new randomly infected individuals and the SEIRD-state of the population inherited from the previous wave, Eq. (13). To obtain a longitudinal metric, the average activity levels $\bar{A}_{V_{SC}}$ of the supply chains in the

three consecutive epidemic waves are aggregated according to the harmonic mean:

$$\text{LSL} \quad = \quad n_{\text{waves}} \left(\sum_{w \in \{\text{waves}\}} \left(\bar{A}_{V_{SC}|_{w,CS}} \right)^{-1} \right)^{-1} \tag{7}$$

A higher value of LSL indicates a better resistance of the supply chain to failure during epidemic outbreaks.[5] The LSL, as defined, is a longitudinal metric that only depends on the spreading of the supply chain (*spread value*), and the control strategy profile (CS).

Epidemic contact layer. The Person-person social-contact networks are obtained by contracting the daily trajectories of the individuals over shared spatial locations (like 'home', 'sports venue', 'work',...). Our models use a (fast) algorithm to produce artificial networks that closely mimic 'person-person' contact networks $\mathscr{G}(V_{\mathscr{G}}, E_{\mathscr{G}})$ (see detailed explanations in (Broekaert et al., 2024c, 2022) and Appendix A).

The probabilistic SEIRSD-model describes each individual with *probabilities* for the *characteristics* of being 'Susceptible', 'Exposed', 'Infectious', 'Recovered' and 'Dead'. Each node hence is provided with a state vector with the five defining probabilities

$$\mathbf{\Pi}_k(t) = (p_{S,k}(t), p_{E,k}(t), p_{I,k}(t), p_{R,k}(t), p_{D,k}(t)), \tag{8}$$

where the index k runs over all individuals of the population of size N. By regrouping the component for each characteristic, the formalism can be expressed on N-dimensional SEIRD-characteristic vectors

$$\mathbf{p}_X(t) = (p_{X,1}(t), \cdots, p_{X,N}(t)) \tag{9}$$

for all characteristics $X \in \{S, E, I, R, D\}$. The precise diffusion dynamics

[5] The Service Level in a supply chain is linked to the proportion of time nodes spend in the Recovered and Susceptible states, indicating their normal functioning ability. Alternatively, the Service Level of a supply chain over a period T and with nodes in the subset V_{SC}, can be calculated as the average R+S probability, given by: $SL_{V_{SC}}(T) = \frac{1}{|V_{SC}|} \sum_{k \in V_{SC}} \frac{1}{T} \int_0^T p_{R_k}(t)\, dt$ Within the time range of an epidemic wave, a chosen period of the operational cycle T may not monitor the worst impact of the epidemic.

of the disease over the network follows governing equations for the vectors $\mathbf{p}_X(t)$. The details of this dynamical system are explained in Appendix B, and have been reported and tested in our studies (Broekaert et al., 2024b,c, 2022).

Three consecutive epidemic waves are considered, each characterized by different infectivity rates ($\beta_{Med.} \rightarrow \beta_{High} \rightarrow \beta_{Low}$) and varying asymmetric numbers of infectious seeds. This approach simplifies the formal representation of the SEIRSD model by encompassing all infected individuals in a single category I, rather than tracking each across multiple waves. The transition between epidemic waves is maintained within the original five-dimensional SEIRD-state by fractionally reassigning each category and reseeding infections.

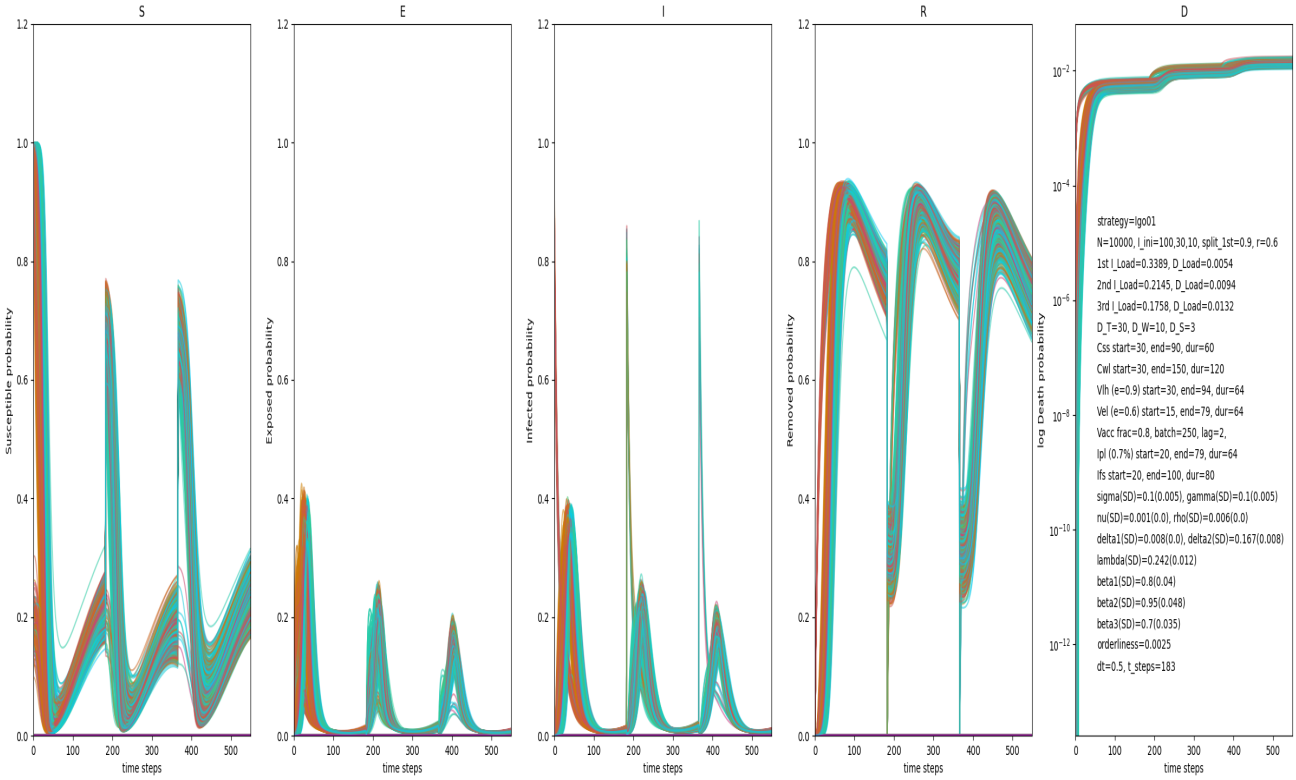

Figure 2: Three consecutive epidemic waves in an uncontrolled SEIRSD epidemic on a designed contact network. The 'Susceptible', 'Exposed', 'Infectious', 'Recovered', and 'Dead' probabilities are shown for each node in the consecutive panels. (orange hues for group_0 and blue hues for group_1)

SC under epidemic controls Subsequent epidemic waves are initialized using the Igo_{01} isolation outcome-state, or 'none_0 none_1' profile, representing the worst-case scenario of an uncontrolled epidemic. Given the number of possible control policy chains $(3 \times 9 \times 9)^3$ and the rescaling and reseeding method, a sufficient trace of inheritance is retained by defaulting to the Igo_{01} outcome. Country isolation policies such as Ifs_{01} and Ipl_{01} may

offer effective control under important asymmetric seeding of the initial infection.

Our study's primary goal is to assess supply chains' resilience and viability through SEIRD-based metrics. Supply chains in the multiplex network are configured by randomly selecting $l_{SC} = 100$ nodes into a co-activity unit, avoiding bias in the results.[6] To evaluate the effect of competing epidemic control policies on supply chain resilience and viability, the spread of supply chain nodes across two regions (populations) is varied. Our model considers five supranational spreads of the supply chains, *spread value* $\in (0, .25, .5, .75, 1)$, representing different fractions of nodes distributed in population_0 and complementarily in population_1.

In addition to confinement strategies, our model now includes isolation strategies that reduce or cut social contact between the two groups. This 'frontier closing' control can implemented with three pre-defined isolation amplitudes: i) no limitations on foreign contacts or, *'freely **go**'* (Igo_{01}), ii) a limitation to only essential cross-border contacts over a longer period, i.e. '***p**artial **l**onger isolation*' (Ipl_{01}), and iii) a total cut-off of all foreign contacts over a limited period, i.e. *'**f**ull but **s**hort isolation*' (Ifs_{01}). These isolation controls augment the previously implemented strategies: 'none', strict short or weak long confinement (Csl and Cwl), and early less effective or late highly effective vaccination (Vel or Vlh), and their combinations. Since isolation control is mutual between regions, the game matrix reduces to three matrices of size 9x9. To reduce the concomitant complexity of possible parametrizations, we implement two basic contact confinement strategies '***s**trict isolation & **s**hort duration*' (Css) versus '***w**eak isolation & **l**ong duration*' (Cwl), and two basic vaccination strategies '***e**arly deployment & **l**ower-efficacy vaccination*' (Vel) versus '***l**ater deployment & **h**igher-efficacy vaccination*' (Vlh), or any possible hybrid of both, or none, of the confinement and vaccination strategies. (the parameters of the strategies are provided in experimental Section 5). Considering the availability of each control strategy, separately or combined, and considering the default or 'no-control'-option, nine possible

[6] In real-world situations the historic emergence of supply chains is based on cost and time optimization, production and stock effectivity, trust, and business acumen.

strategies, can be enumerated and can be deployed by each sub-population,

$$CS = \begin{bmatrix} \text{none} \\ \text{Css} \\ \text{Cwl} \end{bmatrix} \otimes \begin{bmatrix} \text{none} \\ \text{Vel} \\ \text{Vlh} \end{bmatrix} \otimes \begin{bmatrix} \text{Igo}_{01} \\ \text{Ifs}_{01} \\ \text{Ipl}_{01} \end{bmatrix} \tag{10}$$

and are kept fixed in the reported (*ad hoc*) order for identification in the game matrices. The three *isolation* strategies can only be deployed symmetrically between the two policymakers. Besides an insight into a purely epidemic mitigation, the crossing of control strategies in this setting leads to $3 \times 9 \times 9$ *Epidemic Control Cost* expressions for each subpopulation. The shorthand notation for strategy profiles derived from Eq. (10) enable to quickly identify what health measures are deployed by whom. A confinement type starts with C, vaccination with V and isolation type with I. Indices 0 or 1 indicate whether a health measure is deployed for individuals under the policymaker from 'country 0' or 'country 1'. In the short hand notation the health measure by policymaker 0 (1) appear to the left (right). The isolation measures always carry an index 01 as these are deployed symmetrical by definition and these always appear at the end of the short hand notation. For example, the strategy profile $\text{Css}_0\text{\_Vel}_0\text{\_Cwl}_1\text{\_Vel}_1\text{\_Ifs}_{01}$ implies policymaker 0 specifically deploys a 'strict and short' confinement and an 'early and with lower efficacy' vaccination, while policymaker 1 specifically deploys a 'weak and long' confinement and also the 'early and with lower efficacy' vaccination. Besides, both policymakers also deploy the country 'full and short' isolation. The specific parametrization of the control strategies depends on the longitudinal development and the magnitude of the uncontrolled epidemic. The effectiveness of a deployed epidemic control strategy will always be assessed relative to the cost and impact of the uncontrolled epidemic, i.e. Igo_{01} in terms of the listed strategies Eq.(10).

The epidemic evolution is guided by policymakers' control policies. The optimal strategic profile, derived from the cost-based Nash Equilibrium in the game matrix, provides a reference point for supply chain managers for further planning. A manager's perspective on supply chain resilience may lead to different insights into the best control profile and supply chain spread. Our model derives the Nash equilibrium for TTR for each epidemic wave and supply chain *spread value* assessing convergences and divergences between policymaker and supply chain manager resilience-based perspectives.

Supply chain viability is monitored through the harmonic mean activity, or LSL, over the three epidemic waves. A critical assessment is made of the repercussions of policymakers' control policies on supply chain viability, considering their different international structures.

Epidemic Control Cost - Using SEIRD-loads for ECC. Our study aims to compare the cost-optimal control policies for two inter-dependent regions with strategic profiles that emerge from optimizing resilience and viability of supply chains. The Epidemic Control Cost compounds the cost of epidemic health policy, the control strategy, and loss of productivity (see Charpentier et al. (2020); Reddy et al. (2021); Gros et al. (2021); Gollier (2021)). The epidemic costs are correlated with the severity of the epidemic in various ways and will be forecast on epidemic model variables. In contrast with time-integrated epidemic characteristics, *SEIRD-loads* capture potential break-points as these do not correlate to time-averaged metrics. The policymaker's control strategies and their specific parameterization will often depend on worst-case scenarios in the longitudinal development of the epidemic variables. The *SEIRD-loads* are formalized to capture the *worst impact* of the epidemic on a characteristic over the longitudinal time range:

$$X_{\text{load}} \quad = \quad \frac{1}{N} \sum_{j \in V_{\mathscr{G}}} \max_{t} \left(p_{X_j}(t) \right), \quad \forall X \in \{S, E, I, R, D\}. \tag{11}$$

The observed and forecast SEIRD-loads, Eq.(11), in each of the populations, typically the I-load and D-load, will trigger epidemic containment efforts following governmental policy.
The policy impact assessment requires that the implemented control strategies share the exact same underlying reference epidemic and contact network, while the parameters of the confinement and vaccination modalities of a control strategy remain fixed over their various combinations, Eq.(10). The detailed expression of the ECC was reported in our studies (Broekaert et al., 2024c) and in Appendix C. Our model mainly emphasizes four cost components related to the epidemic;

(i) Deployed Control Strategy Costs: This includes the development and production of vaccination technology, its deployment, and the implementation of confinement policies. Costs are influenced by the duration and severity of restrictions and are adjusted for GDP differ-

ences between countries.

(ii) Epidemic-Related Health Policy Deployment Costs: Initially proportional to the infection load, these costs increase when healthcare capacity is exceeded. The model uses a piecewise linear function to represent cost transitions, accounting for the expansion of healthcare facilities and their operational costs.

(iii) Value of Human Life (Death Toll): The costs associated with deceased individuals are proportional to the death count.

(iv) Epidemic-Related Loss of Economic Productivity: Using a Cobb-Douglas production function, the model estimates productivity loss based on reduced labor force participation due to the epidemic.

The SEIRD load-based total incurred epidemic cost, ECC_α for each subpopulation α on the graph of two countries $\alpha \in \{0, 1\}$ is given by

$$ECC_\alpha = c_{\mathrm{cs},\alpha} + c_{I,\alpha}\mathscr{I}(I_\alpha, I_{max\alpha}) + c_{D,\alpha}D_\alpha + c_{L,\alpha}{L_{\max}}^b \left(1\text{-}(1\text{-}E_\alpha\text{-}I_\alpha\text{-}D_\alpha)^b\right) \quad (12)$$

where $c_{I,\alpha}$ represents the cost of disease-related health policy, $c_{\mathrm{cs},\alpha}$ is the implementation cost of the control strategy, $c_{D,\alpha}$ is the cost of deceased individuals, and $c_{L,\alpha}$ is the impact on economic productivity loss.

The proportionality factors of cost are expressed relative to annual GDP per capita following Gros et al. (2021) (Appendix C). The population-specific implementation cost of their control strategy, $c_{\mathrm{cs},\alpha} \in \mathbb{R}$, $\alpha \in \{0, 1\}$ and $\mathrm{cs} \in CS$, is separated along confinement, vaccination and isolation types and directly summed when strategies are combined. The simulation is implemented for two subpopulations with a GDP difference factor $(1 - \mathrm{GDP}_{\mathrm{diff}})$, where $\mathrm{GDP}_{\mathrm{diff}} = .1$. Subpopulation 1 is the reference, and subpopulation group-0 is corrected for its limited resources by a factor $(1 - \mathrm{GDP}_{\mathrm{diff}})$. The cost of intervention from the implemented control strategy, $c_{\mathrm{cs},\alpha}$, is scaled by $CS_{\mathrm{scale}} = 1.5$. Based on Gollier (2021), the relative cost CV_{ratio} of deploying a confinement strategy versus a vaccination strategy $CV_{\mathrm{ratio}} = .1$, here. The cost correlation factors are taken equal $c_I = c_L$. The parameters of the confinement strategy impact its operation cost. The relative confinement duration and severity of contact reduction are implemented as proportional factors, with a lower operation cost in the country with a relatively lower GDP. Formally, the confinement severity is expressed

as a relative deviation from the average number of contacts under normal circumstances without an epidemic in c_{Css}, c_{Cwl}, $c_{\text{Ifs}_{01}}$ and $c_{\text{Ipl}_{01}}$.
The operation and development cost of the vaccination strategy,c_{Vel}, c_{Vlh}, is expressed on its time of launch and effectivity. This framework now allows for the numerical assessment the deployment cost of all crossed control strategies, purely based on SEIRD-loads. In contrast to an optimization approach targeting the minimum of the *time-integregated* cost, the identification of the optimal strategy results from the Nash equilibrium analysis of the game matrix of *SEIRD load-based* costs for all crossed strategies.

4. Methodology and simulation algorithms

Formalism. The simulated network is conceived as a contact graph $\mathscr{G}(V_{\mathscr{G}}, E_{\mathscr{G}})$ spanned on $N = 10^4$ nodes of $V_{\mathscr{G}}$ and with dynamical adjacency, which enables the diffusion of the disease across all contacts $E_{\mathscr{G}}$. Both the specific topology of the social contact network (Appendix A) and the probabilistic SEIRSD evolution (Appendix B have been modeled to reflect real-world contact structure (Barrett et al., 2009) and COVID-19 parametrization (Broekaert et al., 2024c). From a technical perspective, several modifications have been made to the model. An adjacency algorithm based on contact probability exponential decay is implemented to realistically simulate contact networks, allowing for large networks. A faster time pace of epidemic evolution ($dt = .5$) is used, reducing computation time without sacrificing accuracy. Following input initialization for each control configuration, the main algorithm is the Euler-forward method to numerically solve the coupled ODE system, Eqs. (B.1), by using an updated infinitesimal propagator with each time increment, see Fig. 3. Over three epidemic waves, the resulting SEIRD-histories ($3 \times 3 \times 9 \times 9$) then serve to obtain the SEIRD-loads and activity histories of all supply chains with different spreading over the two populations. These allow to calculate the ECC, TTR and LSL following which their Nash equilibria strategy profiles can be obtained.

Epidemic wave sequence At the onset of each new wave, all node states are re-evaluated concerning the new virus variant. The transitions between

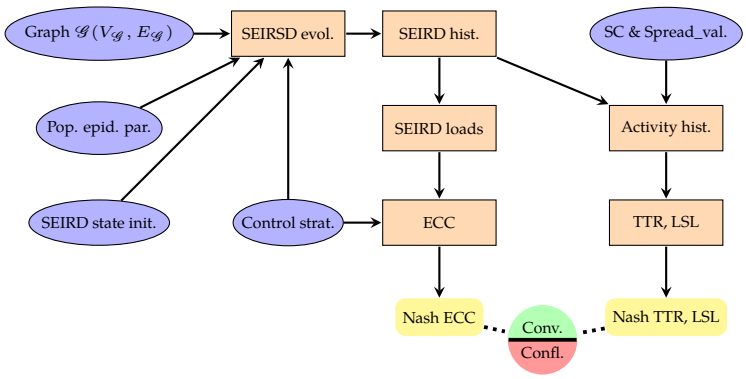

Figure 3: Formal flow of algorithms and methods to analyze conflicts and convergences in epidemic control policies for ECC and resilience and viability of supply chains.

waves are formalized according to the single-time step evolution:

$$\Pi_k(T+dt) \;=\; (1 - V_{Ik}) \begin{bmatrix} p_{S_k} + r_k(p_{E_k} + p_{I_k} + p_{R_k}) \\ (1-r_k)p_{E_k} \\ (1-r_k)p_{I_k} \\ (1-r_k)p_{R_k} \\ p_{D_k} \end{bmatrix}_{(T)} + V_{Ik} \begin{bmatrix} (1 - r_I) - p_{D_k} \\ 0 \\ r_I \\ 0 \\ p_{D_k} \end{bmatrix}_{(T)} \tag{13}$$

where V_I is a random vector indicating infection seeds $(0$ or $1)$ with a fixed number and (as)symmetry, r_I is the infection probability of the seed, and $(p_{S_k}, p_{E_k}, p_{I_k}, p_{R_k}, p_{D_k})_{(T)}$ is the output state vector of node k from the previous wave under the 'Igo$_{01}$' control. Nodes in the population evolve by inheriting scaled characteristics or by seeding with the new virus in limited cases. Recovered individuals become largely susceptible again, with a fraction r_k (e.g., 70%) of p_{R_k} pooled back with p_{S_k} for each node k. The value r_k is sampled from a truncated normal distribution for each node. Exposed and infected characteristics are similarly reduced and pooled with S, renewing sensitivity to the new virus. The number of infective seeds changes over the waves, 100 in the first, 30 in the second, and 10 in the third, reflecting the unexpected nature of the first wave and improved anticipation in subsequent waves. Seeding initially occurs asymmetrically to suggest a dominant source in only one of the populations. The Dead characteristic remains an absorbing state, with p_D invariant during new virus introductions.

Vaccination In our present model, the vaccination state vector is implemented according to:

$$\Pi_k(t+dt) = (1-e)\,\Pi_k(t) + e\ (0,0,0,1-p_{Dk}(t), p_{Dk}(t))\,.$$

This equation weights the successful vaccination outcome state with efficiency e and retains the old node state vector with weight $(1-e)$.
Finally, our model applies truncated normal distributions to all demographic parameters, including r_k, the reset parameter of the SEIRD node-state at the start of the next epidemic wave, and r_{I_k}, the infection rate of the infected seeds causing the next wave.
Model parametrization The numerical simulation entails fixing parameters in the various inputs of the model identified in Fig. 3. The parameter values are listed in Table 1.

Table 1: Model parameter values for the numerical simulation.

Epidemic Parameters	init_infected_1 = 100, init_infected_2 = 30, init_infected_3 = 10, ini_rate = 0.8, split_infect = 0.9, beta_bulk_1 = 0.8, beta_bulk_2 = 0.95, beta_bulk_3 = 0.7, delta1 = epsilon * 1/4, delta2 = 1/6, lambdal = (1 - epsilon) * 1/4, nu = 0.001, rho = 1/180, gamma_bulk = 0.1, sigmas_bulk = 0.1, SDfrac = 0.05, r = 0.6, epsilon = 0.03
Adjacency Parameters	D_T = 30, D_W = 10, D_S = 3, D_eow = 60, pMid = 0.5, pEnd = 0.95, weight = 0.9, orderliness = 0.0025
Confinement Parameters	start_C = 30 / (2 * dt), start_Css = start_C, start_Cwl = start_C, dur_Css = 60 / (2 * dt), dur_Cwl = 120 / (2 * dt), end_Css = start_Css + dur_Css, end_Cwl = start_Css + dur_Cwl
Isolation Parameters	frac_isol = 0.7, start_Ifs = 20 / (2 * dt), start_Ipl = 10 / (2 * dt), dur_Ifs = 80 / (2 * dt), dur_Ipl = 160 / (2 * dt), end_Ifs = start_Ifs + dur_Ifs, end_Ipl = start_Ipl + dur_Ipl
Vaccination Parameters	fraction_vaccinated = 0.8, start_Vel = 15 / (2 * dt), start_Vlh = 30 / (2 * dt), vacc_batch = 0.05 * N / 2, steps_lag_V = 4 * dt, steps_lag_Vel = steps_lag_V, steps_lag_Vlh = steps_lag_V, e_Vel = 0.6, e_Vlh = 0.9
Time Parameters	dt = 0.5, T_start = 0, T_end = 365 / (4 * dt)
Cost Parameters	GDP_diff = 0.1, CS_{scale} = 1.5, conf_vacc_ratio = .1, scaleC = conf_vacc_ratio * CS_{scale}, scaleV = CS_{scale}
Supply Chain Par's	l_{SC}= 100, N_{SC}= 10, $spread\_value \in \{0, .25, .5, .75, 1\}$
LSL Parameters	perf_thresh= 0.7

5. Simulation results and discussion

Given their differing objectives, policymakers and supply chain managers exhibit both convergences and conflicts in their choice of optimal

control policies. A comparative analysis of the Nash equilibria based on Epidemic Control Cost (Table 2), TTR (Table 3), and LSL (Table 4) derived from the simulation experiment leads to the following observations. Various conditions of *wave* and *spread value* let multiple Nash equilibria

Epidemic Control Cost			('lower is better')
Epidemic wave	Isolation strategy	Nash profile policymakers 0 vs. 1	Nash equilibria values 0 vs. 1
first	**Igo**$_{01}$*	Css$_1$_Vel$_1$, **Cwl**$_0$**_Vel**$_0$**_Css**$_1$**_Vel**$_1$*	[0.225, 0.205], **[0.225, 0.202]***
	Ifs$_{01}$	Css$_0$_Vel$_0$_Cwl$_1$_Vel$_1$	[0.282, 0.246]
	Ipl$_{01}$	Css$_1$_Vel$_1$, Cwl$_0$_Vel$_0$_Css$_1$_Vel$_1$	[0.287, 0.273], [0.287, 0.271]
second	**Igo**$_{01}$*	**none***	**[0.274, 0.304]***
	Ifs$_{01}$	Cwl$_1$_Vel$_1$	[0.334, 0.368]
	Ipl$_{01}$	none	[0.336, 0.373]
third	**Igo**$_{01}$*	Css$_0$_Css$_1$, **Css**$_0$**_Css**$_1$**_Vel**$_1$*	[0.343, 0.381], **[0.342, 0.381]***
	Ifs$_{01}$	Css$_0$_Css$_1$	[0.404, 0.449]
	Ipl$_{01}$	Css$_0$_Css$_1$	[0.404, 0.449]

Table 2: Policy maker's strategic control Nash equilibria based on Epidemic Control Cost, for consecutive epidemic waves.

profiles occur based on ECC, TTR or LSL. In a two-player zero-sum game, the payoff of the first player is the negative of the payoff of the second player. In contrast, a non-zero-sum game, as exemplified in our current model, can yield multiple Nash equilibria due to the dissimilar bimatrix payoffs. The study by (Punniyamoorthy et al., 2023) proposes multi-criteria methods to select an optimal Nash equilibrium when multiple options are available. In this case, a heuristic is applied here which selects the *improved values for both players*.

Initial observations reveal that the Nash ECC rises over the consecutive epidemic waves, and tends to be lower for region_0 compared to region_1 – except during the first one, Table 2. This trend aligns with the accumulated death toll (D), while the latter exception is attributed to the initial asymmetrical and dominant infection seeding in region_0 during the first wave (see Table 1). In the first wave, the Nash profile suggests a vaccination campaign – **Vel** in both regions. However, in the second and third waves, driven by new viral strains, policymakers largely abandon vaccination efforts, except in economically stronger region_1 during the third wave (Vel$_1$). Throughout all waves, policymakers opt against restricting inter-regional contacts. In stark contrast, supply chain managers prioritize maintaining competitive TTR and LSL, leading them to prefer isolating contacts between the two

Time To Recovery ('lower is better')

Wave	Spread value	Isolation	Nash profile SC managers 0 & 1	Nash values 0 & 1
first	0.00	**Igo_{01}**⋆	**Css_0_Vel_0_Cwl_1_Vel_1**⋆	**[35.7, 33.0]**⋆
		Ifs_{01}	Css_0_Vel_0_Cwl_1_Vlh_1,...	[42.0, 32.5], ...
		Ipl_{01}⋆	**Css_0_Vel_0_Cwl_1_Vel_1**⋆	**[35.7, 33.0]**⋆
	0.25	Igo_{01}	Css_0_Vel_0_Cwl_1_Vel_1, Vel_0_Css_1_Vel_1	[35.9, 34.0], [37.2, 35.2]
		Ifs_{01}⋆	**Cwl_0_Vel_0_Cwl_1_Vel_1**⋆	**[35.2, 34.0]**⋆
		Ipl_{01}	Css_0_Vel_0_Cwl_1_Vel_1, Vel_0_Css_1_Vel_1	[35.9, 34.0], [37.2, 35.2]
	0.50	Igo_{01}	Css_0_Vel_0_Cwl_1_Vel_1	[34.7, 34.7]
		Ifs_{01}⋆	**Css_0_Vel_0_Cwl_1_Vel_1**⋆	**[34.0, 34.0]**⋆
		Ipl_{01}	Css_0_Vel_0_Cwl_1_Vel_1	[34.7, 34.7]
	0.75	Igo_{01}	Css_0_Vel_0_Cwl_1_Vel_1	[34.0, 35.9]
		Ifs_{01}⋆	**Css_0_Vel_0_Cwl_1_Vel_1**⋆	**[33.9, 35.3]**⋆
		Ipl_{01}	Css_0_Vel_0_Cwl_1_Vel_1	[34.0, 35.9]
	1.00	Igo_{01}	Css_0_Vel_0_Cwl_1_Vel_1	[33.0, 35.7]
		Ifs_{01}⋆	**Css_0_Vel_0_Cwl_1_Vel_1**⋆	**[32.7, 35.0]**⋆
		Ipl_{01}	Css_0_Vel_0_Cwl_1_Vel_1	[33.0, 35.7]
second	0.00	Igo_{01}	Vlh_0_Css_1_Vel_1, Css_0_Vel_0_Css_1_Vlh_1	[30.7, 41.6], [33.9, 30.2]
		Ifs_{01}⋆	**Cwl_0_Vel_0_Cwl_1_Vel_1**⋆, ...	**[30.1, 30.0]**⋆, ...
		Ipl_{01}	Vlh_0_Css_1_Vel_1, Css_0_Vel_0_Css_1_Vlh_1	[30.7, 41.6], [33.9, 30.2]
	0.25	Igo_{01}	Css_0_Vel_0_Cwl_1_Vel_1	[31.0, 30.7]
		Ifs_{01}⋆	**Cwl_0_Vel_0_Cwl_1_Vel_1**⋆	**[30.6, 30.6]**⋆
		Ipl_{01}	Css_0_Vel_0_Cwl_1_Vel_1	[31.0, 30.7]
	0.50	Igo_{01}	Css_0_Vel_0_Cwl_1_Vel_1	[30.7, 30.7]
		Ifs_{01}⋆	**Css_0_Vel_0_Cwl_1_Vel_1**⋆	**[30.5, 30.5]**⋆
		Ipl_{01}	Css_0_Vel_0_Cwl_1_Vel_1	[30.7, 30.7]
	0.75	Igo_{01}	Css_0_Vel_0_Cwl_1_Vel_1	[30.7, 31.0]
		Ifs_{01}⋆	**Css_0_Vel_0_Cwl_1_Vel_1**⋆	**[30.2, 31.0]**⋆
		Ipl_{01}	Css_0_Vel_0_Cwl_1_Vel_1	[30.7, 31.0]
	1.00	Igo_{01}	Css_0_Vel_0_Cwl_1_Vel_1	[30.4, 30.7]
		Ifs_{01}⋆	**Cwl_0_Vel_0_Cwl_1_Vel_1**⋆	**[30.0, 30.1]**⋆
		Ipl_{01}	Css_0_Vel_0_Cwl_1_Vel_1	[30.4, 30.7]
third	0.00	Igo_{01}	Css_0_Vel_0_Cwl_1_Vlh_1, Cwl_0_Vlh_0_Css_1_Vel_1	[32.2, 29.0], [28.8, 32.1]
		Ifs_{01}⋆	**Cwl_0_Vel_0_Css_1_Vlh_1**⋆, ...	**[30.9, 28.7]**⋆, ...
		Ipl_{01}	Css_0_Vel_0_Cwl_1_Vlh_1, Cwl_0_Vlh_0_Css_1_Vel_1	[32.2, 29.0], [28.8, 32.1]
	0.25	Igo_{01}	Css_0_Vel_0_Cwl_1_Vel_1, Cwl_0_Vel_0_Css_1_Vel_1	[29.5, 29.5], [29.3, 29.5]
		Ifs_{01}⋆	**Cwl_0_Vel_0_Css_1_Vel_1**⋆	**[29.0, 29.2]**⋆
		Ipl_{01}	Css_0_Vel_0_Cwl_1_Vel_1, Cwl_0_Vel_0_Css_1_Vel_1	[29.5, 29.5], [29.3, 29.5]
	0.50	Igo_{01}	Css_0_Vel_0_Cwl_1_Vel_1, Cwl_0_Vel_0_Css_1_Vel_1	[29.4, 29.4], [29.4, 29.4]
		Ifs_{01}⋆	**Cwl_0_Vel_0_Cwl_1_Vel_1**⋆	**[29.1, 29.1]**⋆
		Ipl_{01}	Css_0_Vel_0_Cwl_1_Vel_1, Cwl_0_Vel_0_Css_1_Vel_1	[29.4, 29.4], [29.4, 29.4]
	0.75	Igo_{01}	Css_0_Vel_0_Css_1_Vel_1	[29.5, 29.4]
		Ifs_{01}⋆	**Cwl_0_Vel_0_Css_1_Vel_1**⋆	**[29.2, 29.0]**⋆
		Ipl_{01}	Css_0_Vel_0_Css_1_Vel_1	[29.5, 29.4]
	1.00	Igo_{01}	Css_0_Vel_0_Css_1_Vel_1	[29.1, 29.1]
		Ifs_{01}⋆	**Cwl_0_Vel_0_Css_1_Vel_1**⋆	**[28.8, 28.7]**⋆
		Ipl_{01}	Css_0_Vel_0_Css_1_Vel_1	[29.1, 29.1]

Table 3: Manager's strategic control Nash Equilibria based on Time To Recovery (TTR) to regain an activity threshold of .70, for epidemic waves and possible supply chain spread over the two populations (Spread Value).

regions ($\mathbf{Ifs}_{01}$). [7]

the supply chain's TTR-based Nash strategy successfully reduces recovery time across epidemic waves by selecting control profiles that sustain higher activity levels of the nodes. Despite the increased infectiousness of β_2, but fewer infectious seeds, a full outbreak of the epidemic is mitigated. For the interpretation of the supply chain's LSL-based Nash profiles for different spread values one needs to read the entries according to complementary spreading for region_0 and region_1. This implies that region_0's supply chain with *spread value = val* competes with region_1's supply chain with *spread value = 1 - val*.
The LSL Nash for *spread value*=0 shows a high LSL=.763 for a supply chain fully in region_1, and a lower LSL=.675 for a supply chain fully in region_0. Clearly, in the case of supply chains fully contained in one region, the LSL is sensitive to the impact of the first wave that -by design- dominantly struck region_0. In contrast, supply chains with a balanced spread of .5 over both regions reach an LSL Nash of .722 each, showing the advantage of risk spreading by delocalising supply chain nodes.

By comparing the Nash equilibria in Tables 2 (ECC), 3 (TTR, and 4 (LSL), several conflicts and convergences between the policy makers (players 0 and 1) and supply chain managers can be identified.
Control Conflicts: comparing optimal strategies based on Epidemic Control Cost and Time To Recovery reveals that policymakers consistently prefer the Igo_{01} strategy (2) across waves, while supply chain managers favor Ifs_{01} isolation (3). Only during the first epidemic wave, when seeding is asymmetric in group_0, does a Spread Value zero supply chain manager -i.e. fully active in group 1– prefer no-isolation strategy or a partial-longer one (Ipl_{01}). Furthermore, comparing ECC-based strategies with LSL-based ones shows, across all waves, that the policymakers' preferred isolation strategy (Igo_{01}) does not align with those maximizing LSL for supply chain

[7] The only exception to this general preference for $\mathbf{Ifs}_{01}$ is during the *first* wave and uniquely for SC with $spread\_value = 0$, hence fully located in region_1, in which case the TTR-based Nash prescribes $\mathbf{Igo}_{01}$ or $\mathbf{Ipl}_{01}$ with both delivering the numerically same outcome. Due to the high asymmetry of infectious seeding during wave one in region_0 the *isolation* may play no role on the TTR of the SC fully concentrated in region_0, while it would for degrading those in region_1. (Note that the LSL-based Nash does not show this discrepancy, because the previous effect is harmonically averaged out over consecutive waves.)

managers, Ifs_{01} consistently renders higher LSL across various Spread Values. All TTR and LSL Nash equilibria invoke four control components -a confinement and vaccination variant for each group– and an isolation strategy: the implementation cost of the policies tends to tone down the approach of the policymaker's ECC Nash equilibria.

Control Convergences: In the first wave's asymmetric configuration, supply chains with Spread Value = 0 convergence on the Igo_{01} strategy, aligning policymakers with supply chain managers aiming for lower TTR.

In the epidemically weaker third wave, for balanced supply chains (Spread Value = 0.5) both policymakers and supply chain managers again converge on the Igo_{01} strategy. Clearly, a control conflict between policymaker's and supply chain manager's preferred policies appears in the deployment of confinement and vaccination policies. The increased cost implications of deploying vaccination consistently contrast with the TTR-based and LSL-based benefits for the performance of the supply chains. Specifically for region_0 with lower GDP, the vaccination control is only applied in the worst epidemic wave (first wave). Also on the use of the confinement con-

Longitudinal Service Level ('higher is better')

Spread Value	Isolation Type	Nash profile SC managers 0 & 1	Nash values 0 & 1
0.00	Igo_{01}	Css_0_Vel_0_Css_1_Vel_1	[0.759, 0.657]
	Ifs_{01}*	Vlh_1	[0.579, 0.532]
		Cwl_0_Cwl_1	[0.540, 0.544]
		Vlh_0	[0.543, 0.543]
		Vlh_0_Vlh_1	[0.579, 0.543]
		Css_0_Vel_0_Cwl_1_Vel_1*	**[0.763, 0.675]***
	Ipl_{01}	Css_0_Vel_0_Css_1_Vel_1	[0.759, 0.657]
0.25	Igo_{01}	Css_0_Vel_0_Css_1_Vel_1	[0.729, 0.667]
	Ifs_{01}*	**Css_0_Vel_0_Css_1_Vel_1***	**[0.755, 0.683]***
	Ipl_{01}	Css_0_Vel_0_Css_1_Vel_1	[0.730, 0.667]
0.50	Igo_{01}	Css_0_Vel_0_Css_1_Vel_1	[0.701, 0.701]
	Ifs_{01}*	**Css_0_Vel_0_Css_1_Vel_1***	**[0.722, 0.722]***
	Ipl_{01}	Css_0_Vel_0_Css_1_Vel_1	[0.701, 0.701]
0.75	Igo_{01}	Css_0_Vel_0_Css_1_Vel_1	[0.667, 0.729]
	Ifs_{01}*	**Css_0_Vel_0_Css_1_Vel_1***	**[0.683, 0.755]***
	Ipl_{01}	Css_0_Vel_0_Css_1_Vel_1	[0.667, 0.730]
1.00	Igo_{01}	Css_0_Vel_0_Css_1_Vel_1	[0.657, 0.759]
	Ifs_{01}*	**Css_0_Vel_0_Css_1_Vel_1***	**[0.674, 0.788]***
	Ipl_{01}	Css_0_Vel_0_Css_1_Vel_1	[0.657, 0.759]

Table 4: Manager's strategic control Nash Equilibria based on Longitudinal Service Level (LSL), averaged over consecutive epidemic waves and for various spreading of the supply chains over the two regions (Spread Value).

trol policy, some conflicts between both perspectives arise during the second epidemic wave: EEC-based no controls are ordained, while a TTR-aimed control would deploy some confinement measures in both regions.

Effect of Spread Value on Conflicts and Convergences. For Spread Value = 0, the supply chains fully controlled by region_1 show some alignment in the first wave but diverge in subsequent waves as managers prefer Ifs_{01} strategies for lower TTR and higher LSL. The Spread Value = 1, with supply chains fully controlled by region_0, similarly shows initial alignment in the first wave but conflicting approaches in later epidemic waves. For the intermediate Spread Value = 0.50, a full strategic *symmetry* occurs for the ECC and TTR equilibria in the third epidemic wave and the LSL Nash equilibrium. While the precise strategic profile is not the same in each case (ECC, TTR or LSL), the symmetry of the control approach may foster synergetic deployments in both groups and implicitly commends the balanced risk spreading in the supply chain location.

In summary, the Spread Value significantly affects conflict or convergence between policymakers and supply chain managers. Fully controlled supply chains (Spread Value = 0 or 1) exhibit clearer conflict patterns, while intermediate Spread Values introduce a more complex image.

Besides the value for the measure of supranational spreading of supply chains, the economic parameter values in the model determine the ECC, as shown in Appendix C and culminating Eq.(12), within Nash profiles and convergence or divergence of strategies. In our previous work, we pointed out that an estimate of this variability is obtained from the *ECC-elasticity* with model parameters (Broekaert et al., 2024c). While most parameters exhibit an inelastic effect, a shift in Nash Equilibrium may ensue because various control combinations can lead to similar ECC values, as shown in Table D.5.

Practical applicability. Two case studies from the literature illustrate the potential application of our model in real-world scenarios. These cases show how the model can be included to evaluate the resilience of supranational supply chains during epidemics, demonstrating its relevance to both current and historical events. By comparing these real cases with the model's descriptions and predictions, we aim to demonstrate the effectiveness of our proposed work in guiding decision-making for policymakers and supply chain managers.

Case Study 1: The Impact of the COVID-19 Pandemic on Food Retail Supply Chains in Germany. The case study by Burgos and Ivanov (2021) uses

a discrete-event simulation model with anyLogistix to analyze how various pandemic scenarios affected supply chain operations and resilience. It identifies critical factors such as pandemic intensity, government lockdown measures, inventory-ordering dynamics, and shifts in customer behavior. Notably, demand surges and supplier shutdowns significantly impacted supply chain performance, while transportation disruptions had a comparatively lower effect. The network ontology of this study covers ten product categories with three suppliers each (totaling 30) which three distribution centers spread across Germany transport to 28 supermarket locations in five different countries, Germany, Austria, the Czech Republic, Italy, and Hungary. Our individual-based network model with geographic embedding could provide complementary factors to the analysis of the performance of the supranational food retail supply chains. In their 'Scenario 2' –which involves a *shutdown at suppliers' factories* due to labor unavailability– a disease-based impact over time and per network node in the supply chain could provide a more detailed variable for local labor availability per site. This detailed component description could include differing control strategies in Germany's neighboring countries and enable comparative performance analysis of interchanged strands in the supply network.
In 'Scenario 3', which tests the *bottlenecks due to increased border controls*, their study analyzes disruptions to the normal flow of goods transported into the country but does not consider the possible factor of the (partially) reduced virus spread across the border as suggested by our model ontology. Conversely, their inclusion of changed consumer behavior in Scenario 1 –such as a +75% *increase in demand* due to panic buying following the first lockdown, followed by base demand increase of +10%, and +35% for the second wave– could be incorporated into assessing supply chain efficiency in our model.

Case Study 2: Supply chain management of online retailer JD.com during COVID-19. In a case study by Shen and Sun (2023), the authors examine the impact of the COVID-19 pandemic on supply chain resilience in China, focusing on JD.com. They use quantitative operational data to highlight how JD.com adapted its supply chain management in response to exceptional demand and logistical disruptions. Key insights reveal that JD.com's integrated supply chain structure and intelligent platforms were crucial for maintaining resilience. The company's ability to modify delivery procedures and collaborate effectively with various stakeholders –including government and society– provides practical strategies for navigating large-scale

disruptions. Policymaker lockdown measures impacted JD.com's Wuhan (PRC) distribution center, which serves 120 subordinate warehouses in Hubei, Hunan, Jiangxi, and Henan provinces. This prompted JD.com to adapt its functional network and operations. The paralyzed distribution network in Hubei province led to a real-time data-driven redesign. Unavailable paths and downed distribution centers were removed, optimizing their supply network based on costs, turnover duration, and sales. Cost-based reconfigurations of supply chains following control policy-related losses were proposed using the multiplex network ontology in our study Broekaert et al. (2024c): the particular adaptations to their configurations follow the regional control implementations here and provide resilience by exchanging components.

Model constraints and limitations. The ontology of our model is a multiplex network model that integrates social contacts and supply chain activities. However, these components may not adequately account for influential agents in a business system during major disruptions, such as financial markets, investors, or labor migration patterns. Lucas's critique should be considered, as real-world variability and uncertainty during major disruptions may not align with parameter scaling in the predefined historical ontology and its dynamics. The model is specifically tailored for epidemic scenarios and health strategies, requiring adaptation for generalization to other types of disruptions or specific industries. Only the most basic configuration of two regions on a static network was covered. In principle, changing populations with migrations could be considered, which would require information on the transient parts of the network structures. Considering more than two regions or policymakers in the configuration requires extending to multi-player matrix games to identify the Nash equilibrium strategic profile.

Additionally, the focus on supranational supply chains may not address challenges unique to smaller or more localized supply chains. Furthermore, the longitudinal scope for the LSL metric might not fully capture long-term impacts on aspects such as employment or consumer behavior shifts due to prolonged adverse conditions. Our approach primarily involves mostly static policy analysis, with changes in strategic profiles occurring only between epidemic waves. In reality, policies are dynamically adjusted as new information emerges during each epidemic episode. The possibility of synergetic effects from cooperation is not accounted for in the encompassing control costs in our current model. The presented matrix game

neither penalizes asymmetric strategic profiles nor rewards symmetric ones. Synergetic effects from cooperative epidemic control strategies by regional policymakers can arise from several key factors: information sharing enhances the ability to detect and respond to outbreaks collaboratively by mobilizing joint health supply chains, sharing laboratory facilities, training institutions, and emergency stockpiles. These factors could be incorporated by modularly reducing the ECC (Encompassing Control Cost) when control components are deployed symmetrically by policymakers and align with the shared confinement and vaccination types, as listed in Eq. (10). Currently, the complexity of our model's ontology relies on simulated hypothetical data for analysis and heuristics. Real-world data should provide more accurate insights, but such data may not be available at the same level of detail and may not easily inform the model's parametrization.

6. Conclusions

Our study addresses the critical intersection of supply chain management and public health policy during epidemic scenarios. We developed a comprehensive model that integrates an individual-based multiplex network ontology and a probabilistic SEIRSD-dynamic framework to evaluate the resilience and viability of supranational supply chains under various control strategies. Our model complements existing literature by incorporating detailed cost components and leveraging Nash equilibrium analysis for performance metrics to identify optimal control strategies.

The problem of balancing supply chain performance with public health control measures has been a challenge, especially highlighted during the COVID-19 pandemic. Our model provides an encompassing approach to this problem by focusing on four primary cost components: deployed control strategy, epidemic-related health policy deployment, value of human life, and epidemic-related loss of economic productivity, and by introducing resilience and viability metrics for supply chains. The costs are adjusted for GDP differences between countries and are influenced by factors such as the duration and severity of restrictions, vaccine efficacy, and healthcare capacity. While the supply chain metrics are specified for different location spreading between groups or regions.

By utilizing the SEIRD-probabilities of the nodes in the supply chain subset V_{SC}, we derived effective metrics for Time To Recovery (TTR) and Longitudinal Service Level (LSL). TTR is estimated based on the time it

takes for a significant proportion of nodes to reach a threshold recovery probability (after minimum performance), while LSL is assessed by harmonically averaging the activity probabilities over time (Susceptible and Recovered). These metrics provide a quantitative approach to understanding and managing supply chain resilience and performance.

Our numerical simulations revealed several key observations:

- Policymakers and supply chain managers often have conflicting optimal strategies, particularly when balancing Epidemic Control Costs (ECC) with TTR and LSL.

- The spread value of supply chains significantly influences the degree of conflict or convergence between policymakers and supply chain managers.

- Intermediate spread values introduce a more complex dynamic, often fostering synergetic deployments and balanced risk spreading in supply chain location.

In our approach, resilience and viability of supply chains are monitored using the robust metrics of TTR and LSL. While these metrics can be easily derived from epidemic state vectors of the individuals in the network, these should be further validated and, also derived in models for major disruptions of non-epidemic nature, while various additional performance metrics could be envisaged. The present model framework could be expanded to integrate real-world data and network structures, enhancing its accuracy and including relevant agents in future developments. These improved models should be adapted dynamically as new data becomes available over time, reaching thresholds or providing measures to update effective policies. An expansion of the model to include other types of disruptions, such as major geopolitical events or global resource depletion, is envisaged to make it more versatile and applicable across different contexts. Previous developments on the psychological effect of infectivity Broekaert et al. (2024a) and preference Broekaert et al. (2022) included human behavior in relation to disease and policies; however, behavioral economics could also demonstrate how individuals and organizations might respond to various control measures beyond purely economic considerations. The generic structure of the supply chains left specifics of different industries with varying structures open, which could provide insights into industry-specific vulnerabilities when adopted, and improve the forecasting of supply chain performance.

In conclusion, our model offers an effective framework for policymakers and supply chain managers to make informed decisions during prolonged

epidemic conditions, ensuring the resilience and viability of supply chains. Continuous monitoring and dynamic policy adjustments based on our metrics can help mitigate the adverse effects of epidemics on supranational supply networks.

References

Ajmal, M. M., Khan, M., and Shad, M. K. (2021). The global economic cost of coronavirus pandemic: current and future implications. *Public Administration and Policy*, 24(3):290–305. *Cited on page 2*

Amir, R. and Boucekkine, R. (2022). Introduction to the special issue on new insights into economic epidemiology: Theory and policy. *Journal of Public Economic Theory*, 24(5):861–872. *Cited on page 2*

Ardolino, M., Bacchetti, A., and Ivanov, D. (2022). Analysis of the COVID-19 pandemic's impacts on manufacturing: a systematic literature review and future research agenda. *Operations Management Research*. *Cited on page 2*

Barrett, C. L., Beckman, R. J., Khan, M., Kumar, V. S. A., Marathe, M. V., Stretz, P. E., Dutta, T., and Lewis, B. (2009). Generation and analysis of large synthetic social contact networks. In *Proceedings of the 2009 Winter Simulation Conference (WSC)*, pages 1003–1014. *3 citations, pages 7, 18, and 34*

Bertozzi, A. L., Franco, E., Mohler, G., Short, M. B., and Sledge, D. (2020). The challenges of modeling and forecasting the spread of covid-19. *Proceedings of the National Academy of Sciences*, 117(29):16732–16738. *Cited on page 2*

Borgatti, S. and Halgin, D. S. (2011). Network theorizing. *Organization Science*, 22(5):1168–1181. *Cited on page 6*

Boucekkine, R., Carvajal, A., Chakraborty, S., and Goenka, A. (2021). The economics of epidemics and contagious diseases: An introduction. *Journal of Mathematical Economics*, 93:102498. *Cited on page 2*

Boucekkine, R. and Laffargue, J.-P. (2010). On the distributional consequences of epidemics. *Journal of Economic Dynamics and Control*, 34(2):231–245. *Cited on page 7*

Broekaert, J. B., La Torre, D., and Hafiz, F. (2022). Competing control scenarios in probabilistic SIR epidemics on social-contact networks. *Annals of Operations Research*, pages 1–24. *4 citations, pages 7, 12, 13, and 29*

Broekaert, J. B., La Torre, D., and Hafiz, F. (2024a). The impact of the psychological effect of infectivity on Nash-balanced control strategies for epidemic networks. *Annals of Operations Research*. *2 citations, pages 7 and 29*

Broekaert, J. B., La Torre, D., Hafiz, F., and Brusset, X. (2024b). The diverging control policy's hand in supranational supply chain reconfiguration. (*submitted*). *3 citations, pages 2, 7, and 13*

Broekaert, J. B., La Torre, D., Hafiz, F., and Repetto, M. (2024c). A comparative cost assessment of coalescing epidemic control strategies in heterogeneous social-contact networks. *Computers & Operations Research*, 167:106680. *8 citations, pages 7, 12, 13, 16, 18, 25, 27, and 39*

Brusset, X., Davari, M., Kinra, A., and Torre, D. L. (2022). Modelling ripple effect propagation and global supply chain workforce productivity impacts in pandemic disruptions. *International Journal of Production Research*, pages 1–20. *Cited on page 6*

Brusset, X., Ivanov, D., Jebali, A., La Torre, D., and Repetto, M. (2023). Supply chain reconfiguration and ripple effect analysis in a pandemic: A dynamic approach. *International Journal of Production Economics*, 263(108935):1–13. *Cited on page 6*

Burgos, D. and Ivanov, D. (2021). Food retail supply chain resilience and the covid-19 pandemic: A digital twin-based impact analysis and improvement directions. *Transportation Research Part E: Logistics and Transportation Review*, 152:102412. *Cited on page 25*

Charpentier, A., Elie, R., Laurière, M., and Tran, V. C. (2020). COVID-19 pandemic control: balancing detection policy and lockdown intervention under ICU sustainability*. *Math. Model. Nat. Phenom.*, 15:57. *2 citations, pages 6 and 16*

Chen, K., Pun, C. S., and Wong, H. Y. (2023). Efficient social distancing during the COVID-19 pandemic: Integrating economic and public health considerations. *European Journal of Operational Research*, 304(1):84–98. *Cited on page 6*

Choi, T.-M. (2021). Fighting against COVID-19: What operations research can help and the sense-and-respond framework. *Annals of Operations Research*. *Cited on page 6*

Chowdhury, M. M. H. and Quaddus, M. (2017). Supply chain resilience: Conceptualization and scale development using dynamic capability theory. *International Journal of Production Economics*, 188:185–204. *Cited on page 5*

da Fonseca, E. M., Shadlen, K. C., and de Moraes Achcar, H. (2023). Vaccine technology transfer in a global health crisis: Actors, capabilities, and institutions. *Research Policy*, 52(4):104739. *Cited on page 7*

Das, S., Bose, I., and Sarkar, U. K. (2023). Predicting the outbreak of epidemics using a network-based approach. *European Journal of Operational Research*, 309(2):819–831. *Cited on page 6*

Dobson, A., Ricci, C., Boucekkine, R., Gozzi, F., Fabbri, G., Loch-Temzelides, T., and Pascual, M. (2023). Balancing economic and epidemiological interventions in the early stages of pathogen emergence. *Science Advances*, 9(21):eade6169. *Cited on page 2*

Dolgui, A., Gusikhin, O., Ivanov, D., Li, X., and Stecke, K. (2024). A network-of-networks adaptation for cross-industry manufacturing repurposing. *IISE Transactions*, 56(6):666–682. *Cited on page 6*
Echefaj, K., Charkaoui, A., Cherrafi, A., and Ivanov, D. (2024a). Design of resilient and viable sourcing strategies in intertwined circular supply networks. *Annals of Operations Research*, 337(1):459–498. *Cited on page 6*
Echefaj, K., Cherrafi, A., Charkaoui, A., Gruchmann, T., and Ivanov, D. (2024b). Firm survivability during long-term disruptions: an adaptation-based view. *Supply Chain Management: An International Journal*, ahead-of-print(ahead-of-print). *Cited on page 5*
Eryarsoy, E., Shahmanzari, M., and Tanrisever, F. (2023). Models for government intervention during a pandemic. *European Journal of Operational Research*, 304(1):69–83. *Cited on page 6*
Falasca, M. and Zobel, C. W. (2008). A decision support framework to assess supply chain resilience. *Cited on page 3*
Fan, J., Yin, Q., Xia, C., and Perc, M. (2022). Epidemics on multilayer simplicial complexes. *Proceedings of the Royal Society A: Mathematical, Physical and Engineering Sciences*, 478(2261):20220059. *Cited on page 6*
Farahani, R. Z., Ruiz, R., and Van Wassenhove, L. N. (2023). Introduction to the special issue on the role of operational research in future epidemics/ pandemics. *European Journal of Operational Research*, 304(1):1–8. *Cited on page 7*
Godio, A., Pace, F., and Vergnano, A. (2020). SEIR modeling of the italian epidemic of sars-cov-2 using computational swarm intelligence. *International journal of environmental research and public health*, 17(10):3535. *Cited on page 2*
Gollier, C. (2021). The welfare cost of vaccine misallocation, delays and nationalism. *Journal of Benefit-Cost Analysis*, 12(2):199–226. *4 citations, pages 7, 16, 17, and 39*
Gros, C., Valenti, R., Schneider, L., Valenti, K., and Gros, D. (2021). Containment efficiency and control strategies for the corona pandemic costs. *Scientific Reports*, 11(1):6848. *4 citations, pages 7, 16, 17, and 38*
Gruchmann, T., Stadtfeld, G. M., Thürer, M., and Ivanov, D. (2024). Supply chain resilience as a system quality: survey-based evidence from multiple industries. *International Journal of Physical Distribution & Logistics Management*, 54(1):92–117. *Cited on page 5*
Hille, K. (2021). Taiwan's Covid-19 outbreak spreads to chip companies. *Financial Times*. *Cited on page 2*
Huberts, N. F. and Thijssen, J. J. (2023). Optimal timing of non-pharmaceutical interventions during an epidemic. *European Journal of Operational Research*, 305(3):1366–1389. *Cited on page 7*
Ivanov, D. (2020). Predicting the impacts of epidemic outbreaks on global supply chains: A simulation-based analysis on the coronavirus outbreak (COVID-19/SARS-CoV-2) case. *Transportation Research Part E: Logistics and Transportation Review*, 136:101922. *Cited on page 6*
Ivanov, D. (2024a). Supply chain resilience: Conceptual and formal models drawing from immune system analogy. *Omega*, 127:103081. *Cited on page 5*
Ivanov, D. (2024b). Transformation of supply chain resilience research through the covid-19 pandemic. *International Journal of Production Research*, 0(0):1–22. *Cited on page 5*
Ivanov, D. (2024c). Two views of supply chain resilience. *International Journal of Production Research*, 62(11):4031–4045. *Cited on page 6*
Ivanov, D. and Dolgui, A. (2020). Viability of intertwined supply networks: extending the supply chain resilience angles towards survivability. a position paper motivated by COVID-19 outbreak. *International Journal of Production Research*, 58(10):2904–2915. *Cited on page 3*
Ivanov, D., Sokolov, B., Chen, W., Dolgui, A., Werner, F., and Potryasaev, S. (2020). A control approach to scheduling flexibly configurable jobs with dynamic structural-logical constraints. *IISE Transactions*, 53(1):21–38. *Cited on page 6*
Jackson, J. K., Weiss, M. A., Schwarzenberg, A. B., Nelson, R. M., Sutter, K. M., and Sutherland, M. D. (2021). Global economic effects of COVID-19. Technical Report R46270, Congressional Research Service. *Cited on page 2*
Juan, S.-J., Li, E. Y., and Hung, W.-H. (2022). An integrated model of supply chain resilience and its impact on supply chain performance under disruption. *The International Journal of Logistics Management*, 33(1):339–364. *Cited on page 5*
Keeling, M. J. and Eames, K. T. (2005). Networks and epidemic models. *Journal of The Royal Society Interface*, 2(4):295–307. *Cited on page 6*
Kermack, W. and McKendrick, A. (1927). A contribution to the mathematical theory of epidemics. *Proceedings of the Royal Society of London series A*, 115(772):700–721. *Cited on page 35*
Kinra, A., Ivanov, D., Das, A., and Dolgui, A. (2020). Ripple effect quantification by supplier risk exposure assessment. *International Journal of Production Research*, 58(18):5559–5578. *Cited on page 6*
Kravchenko, K., Gruchmann, T., Ivanova, M., and Ivanov, D. (2024). Responding to the ripple effect from systemic disruptions: empirical evidence from the semiconductor shortage during covid-19. *Modern Supply Chain Research and Applications*, ahead-of-print(ahead-of-print). *Cited on page 6*
Levin, E. G., Lustig, Y., Cohen, C., Fluss, R., Indenbaum, V., Amit, S., Doolman, R., Asraf, K., Mendelson, E., Ziv, A., Rubin, C., Freedman, L., Kreiss, Y., and Regev-Yochay, G. (2021). Waning immune humoral response to BNT162b2 Covid-19 vaccine over 6 months. *New England Journal of Medicine*, 385(24):e84. *Cited on page 35*
Li, Y. and Zobel, C. W. (2020). Exploring supply chain network resilience in the presence of the ripple effect. *International Journal of Production Economics*, 228:107693. *Cited on page 6*
Llaguno, A., Mula, J., and Campuzano-Bolarin, F. (2021). State of the art, conceptual framework and simulation

analysis of the ripple effect on supply chains. *International Journal of Production Research*. *Cited on page 6*
Lofvers, M. (2020). Three-quarters of European supply chains are negatively impacted by coronavirus. Technical report, Supply Chain Movement, Digital Magazine. *Cited on page 2*
MacIntyre, C. R., Costantino, V., and Trent, M. (2021). Modelling of COVID-19 vaccination strategies and herd immunity, in scenarios of limited and full vaccine supply in nsw, australia. *Vaccine*. *Cited on page 2*
Mishra, D., Dwivedi, Y. K., Rana, N. P., and Hassini, E. (2019). Evolution of supply chain ripple effect: a bibliometric and meta-analytic view of the constructs. *International Journal of Production Research*, 59(1):129–147. *Cited on page 6*
Mosayebi, M., Fathi, M., Hedayati, M. K., and Ivanov, D. (2024). Time-to-adapt (tta). *International Journal of Production Economics*, page 109432. *Cited on page 8*
Nagurney, A. (2021a). Optimization of supply chain networks with inclusion of labor: Applications to COVID-19 pandemic disruptions. *International Journal of Production Economics*, 235:108080. *Cited on page 7*
Nagurney, A. (2021b). Supply chain game theory network modeling under labor constraints: Applications to the Covid-19 pandemic. *European Journal of Operational Research*, 293(3):880–891. *Cited on page 7*
Nagurney, A., Flores, E. A., and Soylu, C. (2016). A generalized Nash equilibrium network model for post-disaster humanitarian relief. *Transportation Research Part E: Logistics and Transportation Review*, 95:1–18. *Cited on page 7*
Newman, M. (2018). *Networks*. Oxford University Press. *Cited on page 6*
Ouardighi, F. E., Khmelnitsky, E., and Sethi, S. P. (2022). Epidemic control with endogenous treatment capability under popular discontent and social fatigue. *Production and Operations Management*. *Cited on page 6*
Park, Y. W., Blackhurst, J., Paul, C., and Scheibe, K. P. (2021). An analysis of the ripple effect for disruptions occurring in circular flows of a supply chain network. *International Journal of Production Research*, pages 1–19. *Cited on page 6*
Paul, S. K., Moktadir, M. A., Sallam, K., Choi, T.-M., and Chakrabortty, R. K. (2021). A recovery planning model for online business operations under the COVID-19 outbreak. *International Journal of Production Research*, pages 1–23. *Cited on page 6*
Peng, K., Lu, Z., Lin, V., Lindstrom, M. R., Parkinson, C., Wang, C., Bertozzi, A. L., and Porter, M. A. (2021). A multilayer network model of the coevolution of the spread of a disease and competing opinions. *Cited on page 6*
Plazas, A., Malvestio, I., Starnini, M., and Díaz-Guilera, A. (2021). Modeling partial lockdowns in multiplex networks using partition strategies. *Applied Network Science*, 6(1):27. *Cited on page 7*
Prasse, B., Devriendt, K., and Van Mieghem, P. (2021). Clustering for epidemics on networks: A geometric approach. *Chaos: An Interdisciplinary Journal of Nonlinear Science*, 31(6):063115. *Cited on page 7*
Punniyamoorthy, M., Abraham, S., and Thoppan, J. J. (2023). A method to select best among multi-Nash equilibria. *Studies in Microeconomics*, 11(1):101–127. *Cited on page 21*
Reddy, K. P., Shebl, F. M., Foote, J. H. A., Harling, G., Scott, J. A., Panella, C., Fitzmaurice, K. P., Flanagan, C., Hyle, E. P., Neilan, A. M., Mohareb, A. M., Bekker, L.-G., Lessells, R. J., Ciaranello, A. L., Wood, R., Losina, E., Freedberg, K. A., Kazemian, P., and Siedner, M. J. (2021). Cost-effectiveness of public health strategies for COVID-19 epidemic control in South Africa: a microsimulation modelling study. *The Lancet Global Health*, 9(2):e120–e129. *2 citations, pages 7 and 16*
Reicher, S. and Stott, C. (2020). On order and disorder during the COVID-19 pandemic. *British Journal of Social Psychology*, 59(3):694–702. *Cited on page 2*
Rozhkov, M., Ivanov, D., Blackhurst, J., and Nair, A. (2022). Adapting supply chain operations in anticipation of and during the covid-19 pandemic. *Omega*, 110:102635. *Cited on page 5*
Ruel, S., El Baz, J., Ivanov, D., and Das, A. (2024). Supply chain viability: conceptualization, measurement, and nomological validation. *Annals of Operations Research*, 335(3):1107–1136. *2 citations, pages 3 and 6*
Saad-Roy, C. M., Wingreen, N. S., Levin, S. A., and Grenfell, B. T. (2020). Dynamics in a simple evolutionary-epidemiological model for the evolution of an initial asymptomatic infection stage. *Proceedings of the National Academy of Sciences*, 117(21):11541–11550. *Cited on page 35*
Salarpour, M. and Nagurney, A. (2021). A multicountry, multicommodity stochastic game theory network model of competition for medical supplies inspired by the covid-19 pandemic. *International Journal of Production Economics*, 236:108074. *Cited on page 7*
Sawik, T. (2022). Stochastic optimization of supply chain resilience under ripple effect: A COVID-19 pandemic related study. *Omega*, 109:102596. *Cited on page 6*
Scarpin, M. R. S., Scarpin, J. E., Krespi Musial, N. T., and Nakamura, W. T. (2022). The implications of COVID-19: Bullwhip and ripple effects in global supply chains. *International Journal of Production Economics*, 251:108523. *Cited on page 6*
Shen, Z. M. and Sun, Y. (2023). Strengthening supply chain resilience during covid-19: A case study of jd.com. *Journal of Operations Management*, 69(3):359–383. *Cited on page 26*
Wong, A. S. Y. and Kohler, J. C. (2020). Social capital and public health: responding to the COVID-19 pandemic. *Globalization and Health*, 16(1):88. *Cited on page 35*
Wu, J., Liang, B.-Y., Fang, Y.-H., Wang, H., Yang, X.-L., Shen, S., Chen, L.-K., Li, S.-M., Lu, S.-H., Xiang, T.-D., Liu, J., Le-Trilling, V. T. K., Lu, M.-J., Yang, D.-L., Deng, F., Dittmer, U., Trilling, M., and Zheng, X. (2021). Occurrence of COVID-19 symptoms during SARS-CoV-2 infection defines waning of humoral immunity. *Frontiers in Immunology*, 12. *Cited on page 35*
Xu, Z., Wu, B., and Topcu, U. (2021). Control strategies for COVID-19 epidemic with vaccination, shield immunity

and quarantine: A metric temporal logic approach. *PLOS ONE*, 16(3):1–20. *Cited on page 2*

Yang, W. (2021). Modeling COVID-19 pandemic with hierarchical quarantine and time delay. *Dynamic Games and Applications*. *Cited on page 2*

Yu, K. D. S. and Aviso, K. B. (2020). Modelling the economic impact and ripple effects of disease outbreaks. *Process Integration and Optimization for Sustainability*, pages 1–4. *Cited on page 6*

Appendices

Appendix A. The social contact algorithm

The typical dense clustering of human social contacts is expressed by the clustering degree of each node k in the graph. Formally the cc is "It is obtained by dividing the number of edges between a vertex's neighbors by the number of edges that could possibly exist." or equivalently by the fraction of all existing triangles through node k and all possible triangles among k's neighbors. Both distributions derived from the artificial networks –from the adjacency creation algorithm– need to show representative values of typical human contact networks (Barrett et al., 2009).

Algorithm 1 Adjacency Creator Function

Function adjacency_creator(N, D_T, D_W, D_S, D_eow, pMid, pEnd, weight)
Generate upper triangular indices for an $N \times N$ matrix
$row\_indices, col\_indices \leftarrow$ generate_upper_triangular_indices(N)
Calculate distances from main and secondary diagonals
$D \leftarrow$ absolute_difference(row_indices, col_indices) {Distance from main diagonal}
$d \leftarrow$ absolute_difference(row_indices + col_indices + 1, N) {Distance from secondary diagonal}
Calculate connection probabilities based on distances
$a \leftarrow \exp\left(\frac{-(N-1-d)}{D\_eow}\right)$ {Probability towards "end of world"}
$b \leftarrow \exp\left(\frac{-(N-2)}{D\_eow}\right)$ {Base probability}
$pDiag \leftarrow pEnd \cdot \left(\frac{a-b}{1-b}\right) + pMid \cdot \left(\frac{1-a}{1-b}\right)$ {Combined probability}
Calculate ordered probabilities for different confinement types
$pOrd\_X \leftarrow pDiag \cdot \exp\left(\frac{-(D-1)}{D\_X}\right), \quad \forall X \in \{T, W, S\}$
$D\_XY \leftarrow \frac{D\_X + D\_Y}{2}, \quad \forall X, Y \in \{T, W, S\}$
$pOrd\_X \leftarrow pDiag \cdot \exp\left(\frac{-(D-1)}{D\_X}\right), \quad \forall X \in \{TW, WS, TS\}$
Shuffle the ordered probabilities to create unordered probabilities
$pUnord\_X \leftarrow$ shuffle_probabilities$(pOrd_X), \quad \forall X \in \{T, W, S, TW, WS, TS\}$
Combine ordered and unordered probabilities using the weight
$delimiter\_X \leftarrow pOrd\_X \cdot weight + (1 - weight) \cdot pUnord\_X, \quad \forall X \in \{T, W, S, TW, WS, TS\}$
Generate candidate random values for probabilistic realization
$candidate \leftarrow$ generate_random_values$(delimiter_T.shape)$
Create probabilistic realizations of adjacency matrices
$proto\_X \leftarrow (candidate < delimiter\_X) \cdot 1, \quad \forall X \in \{T, W, S, TW, WS, TS\}$
Initialize adjacency matrices
$adj\_mat\_X \leftarrow$ proto_X, $\quad \forall X \in \{T, W, S, TW, WS, TS\}$
return $adj\_mat\_T, adj\_mat\_W, adj\_mat\_S, adj\_mat\_TW, adj\_mat\_TS, adj\_mat\_WS$

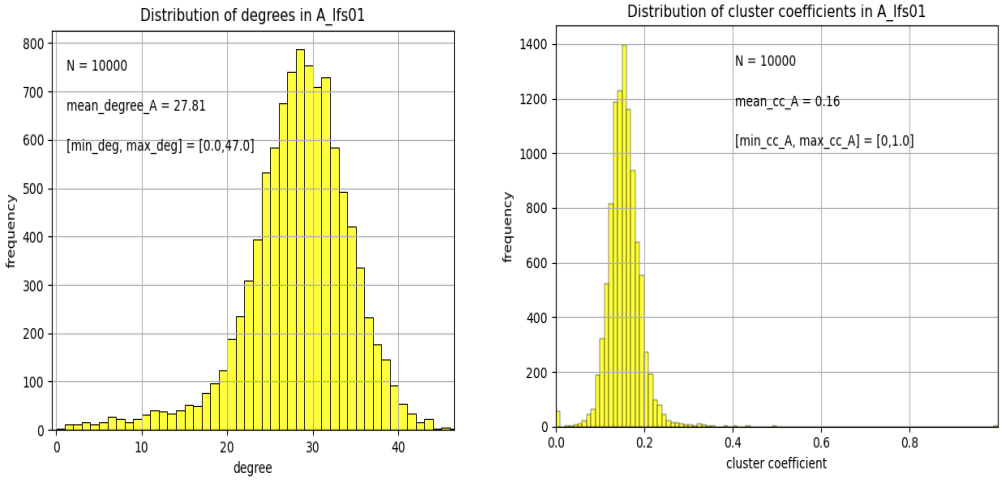

Figure A.4: The distribution of heterogenous social contact degree in the network under strict regional isolation A_Ifs$_{01}$ (left) and the high clustering value of nodes (right).

Appendix B. Epidemic network dynamics

For each node, five probabilities define its state within one of the respective conditions $\{S, E, I, R, D\}$: $\mathbf{\Pi}_k(t) = (p_{S,k}(t), p_{E,k}(t), p_{I,k}(t), p_{R,k}(t), p_{D,k}(t))$. These probabilities can be regrouped into graph-based N-dimensional segment vectors $\mathbf{p}_X(t) = (p_{X,1}(t), \cdots, p_{X,N}(t))$, defined for each characteristic $X \in \{S, E, I, R, D\}$. These probabilities evolve based on the disease's impact on each node's ego-network, which is variable for each individual and includes only those edges of the full graph $E_{\mathcal{G}}$ where the individual is the central node connected to its first neighbors. The adjacency of nodes, represented by the matrix A, is thus a critical factor in the progression of an epidemic.

The individual-based model extends the original approach by Kermack and McKendrick (1927), where the infectious force is proportional to the product of the susceptible (S) and infectious (I) components. Similar product terms have been included for social recovery effects Wong and Kohler (2020) and the impact of re-exposure on immunity loss (Wu et al., 2021), as well as for the observed waning of immunity (Levin et al., 2021; Saad-Roy et al., 2020). The waning immunity effect introduces the possibility of a cyclic trajectory, as the Recovered component can decay back into the Susceptible component, hence the designation 'SEIRSD' network model.

The epidemic system includes the following factors for each node in its governing equations:

1. **($\mathbf{S} \to \mathbf{E}$): Exposure** arises from the infection term $\mathbf{p}_S \circ A(\boldsymbol{\beta}_{\mathscr{G}} \circ \mathbf{p}_I)$, which combines a node's susceptibility with the infectiousness in its ego-network, scaled by β. This corresponds to each node's role as a susceptible 'subject' and 'infector'.

2. **($\mathbf{E} \to \mathbf{I}$ and $\mathbf{E} \to \mathbf{R}$): Disease outbreak** resulting in infection is caused by exposure to the virus, $\boldsymbol{\lambda} \circ \mathbf{p}_E$, and manifests later with latency $\boldsymbol{\lambda}$. The dominant channel-weight of $1 - \varepsilon$ leads to the Infectious state, while a less common channel-weight ε leads to the Recovered state according to the first recovery rate, $\boldsymbol{\delta}_1$.

3. **($\mathbf{I} \to \mathbf{R}$): Basic ('second') recovery** from the disease, $\boldsymbol{\delta}_2 \circ \mathbf{p}_I$, is further enhanced by social support from the ego-network's Recovered component, $\boldsymbol{\delta}_2 \circ \mathbf{p}_I A\boldsymbol{\sigma}_{\mathscr{G}} \circ \mathbf{p}_R$.

4. **($\mathbf{I} \to \mathbf{D}$): Virulence** term $\boldsymbol{\nu} \circ \mathbf{p}_I$ is mitigated by social support strength from the ego-network, $\boldsymbol{\nu} \circ \mathbf{p}_I \circ A(\boldsymbol{\sigma}_{\mathscr{G}} \circ \mathbf{p}_R)$.

5. **($\mathbf{R} \to \mathbf{S}$): Waning immunity** term, $\boldsymbol{\rho} \circ \mathbf{p}_R$, is diminished by re-exposure to the disease in the node's ego-network, $\boldsymbol{\rho} \circ \mathbf{p}_R \circ A(\boldsymbol{\gamma}_{\mathscr{G}} \circ \mathbf{p}_I)$.

These factors lead to the $5 \times N$ coupled governing equations of the graph-based epidemic system:

$$\begin{bmatrix} \dot{\mathbf{p}}_S \\ \dot{\mathbf{p}}_E \\ \dot{\mathbf{p}}_I \\ \dot{\mathbf{p}}_R \\ \dot{\mathbf{p}}_D \end{bmatrix} = \begin{bmatrix} \text{-}\mathbf{p}_S \circ A(\boldsymbol{\beta}_{\mathscr{G}} \circ \mathbf{p}_I) + \boldsymbol{\rho} \circ \mathbf{p}_R \circ (1 \text{ - } A(\boldsymbol{\gamma}_{\mathscr{G}} \circ \mathbf{p}_I)) \\ \mathbf{p}_S \circ A(\boldsymbol{\beta}_{\mathscr{G}} \circ \mathbf{p}_I) \text{ - } (1 \text{ - } \varepsilon)\boldsymbol{\lambda} \circ \mathbf{p}_E - \varepsilon\boldsymbol{\delta}_1 \circ \mathbf{p}_E \\ (1 \text{ - } \varepsilon)\boldsymbol{\lambda} \circ \mathbf{p}_E \text{ - } \boldsymbol{\delta}_2 \circ \mathbf{p}_I \circ (1 + A(\boldsymbol{\sigma}_{\mathscr{G}} \circ \mathbf{p}_R)) \text{ - } \boldsymbol{\nu} \circ \mathbf{p}_I \circ (1 \text{ - } A(\boldsymbol{\sigma}_{\mathscr{G}} \circ \mathbf{p}_R)) \\ \varepsilon\boldsymbol{\delta}_1 \circ \mathbf{p}_E + \boldsymbol{\delta}_2 \circ \mathbf{p}_I \circ (1 + A(\boldsymbol{\sigma}_{\mathscr{G}} \circ \mathbf{p}_R)) \text{ - } \boldsymbol{\rho} \circ \mathbf{p}_R + \boldsymbol{\rho} \circ \mathbf{p}_R \circ A(\boldsymbol{\gamma}_{\mathscr{G}} \circ \mathbf{p}_I) \\ \boldsymbol{\nu} \circ \mathbf{p}_I \circ (1 \text{ - } A(\boldsymbol{\sigma}_{\mathscr{G}} \circ \mathbf{p}_R)) \end{bmatrix} \tag{B.1}$$

It is easily verified that this system conserves the total state probability for each node, as all terms on the right-hand side cancel on summation; $|\boldsymbol{\Pi}_k(t)|_1 = 1, \forall k \in [1 \cdots N], \forall t \in \mathbb{R}^+$.

Appendix C. Epidemic Control Cost

Our model primarily emphasizes four cost components related to the epidemic:

- Deployed Control Strategy: These costs include the development and production of vaccination technology, its deployment, and the implementation costs of confinement policies. Implementing a confinement strategy incurs various costs for policymakers, such as enforcement, logistics, possible compensations, support measures, reorganization of education, and additional social services. A heuristic expression for the cost of confinement considers i) the relative duration of the restriction, ii) the relative severity of contact reduction, and iii) a presumed lower operation cost in lower-GDP countries.
  Similarly, the relative cost of vaccination is evaluated based on i) Vaccine efficacy (e), ii) the relative duration of development and deployment, and iii) the presumed higher investment costs in lower-GDP countries.

- Epidemic-Related Health Policy Deployment: Initially, health costs are proportional to the Infection-load value, serving as a proxy for the number of treated or hospitalized patients. An investment cost is triggered when the projected Infection-load challenges the limited maximal capacity of the health infrastructure (e.g., ICU beds). When the augmented healthcare structure is employed, further day-to-day deployment in that configuration incurs higher proportional costs. These transitions are implemented through a thresholded piecewise-linear expression, $\mathscr{I}(I, I_{max})$, with an initial convex dependency on the expected I-load (under a control strategy) and the uncontrolled I-load, $I_{max} = I_{\text{No-No}}$, when the epidemic ranges freely:

$$\mathscr{I}(I, I_{max}) = \begin{cases} I & : I < I_{max} d_t^{-1} \\ I_{max} d_t^{-1} (1 - f_e) + f_e I & : I_{max} d_t^{-1} < I < I_{max} d_c^{-1} \\ I_{max} \left(d_t^{-1} (1 - f_e) + d_c^{-1} (f_e - f_p) \right) + f_p I & : I > I_{max} d_c^{-1} \end{cases} \tag{C.1}$$

  The fraction of the projected I_{max}-load to trigger augmented facilities is fixed at $d_t = 4$ ('trigger fraction'), and the cost increases by a factor, $f_e = 3$ ('expansion'). This includes refurbishing and stocking medical facilities, occurring well before existing capacity is reached, set at

fraction $d_c = 3$ ('capacity fraction') of the projected I_{max}-load. A cost increase for day-to-day deployment by a factor, $f_p = 1.25$ ('post-operation'), is assumed for yet unreached efficient operation levels.

- Value of Human Life (Death Toll): The private and public costs of deceased individuals are proportional to the death count value.

- Epidemic-Related Loss of Economic Productivity: Assuming constant capital during the epidemic, a Cobb-Douglas production function for economic output is proportional to L^b. The optimal activation in the healthy network is set to the theoretical labor share $L_{max} = 0.9$. Due to the epidemic, the effective activation level in the population diminishes. The probabilistic system state vectors R and S provide the fraction of the network population remaining in a production role. The loss of productivity is proportional to the drop-out $(E+I+D)$ relative to full production capacity.

The defined load-expressions, Eq.(11), longitudinally capture the maximal probabilities to realize the SEIRD characteristics for each node, providing a variable to adequately parametrize various cost instances over the epidemic. Instead of targeting the minimum of the time-integrated cost, the optimal strategy results from the Nash equilibrium analysis of the game matrix of SEIRD load-based costs for all crossed strategies. The SEIRD load-based total incurred epidemic cost for each subpopulation α on the graph of two countries, $\alpha \in \{0, 1\}$, is given by:

$$ECC_\alpha = c_{\mathrm{cs},\alpha} + c_{I,\alpha}\mathscr{I}(I_\alpha, I_{max\alpha}) + c_{D,\alpha}D_\alpha + c_{L,\alpha}{L_{\mathrm{max}}}^b\left(1-(1-E_\alpha-I_\alpha-D_\alpha)^b\right) \quad (12)$$

This equation includes the cost of disease-related health policy $c_{I,\alpha}$, the implementation cost of the control strategy $c_{\mathrm{cs},\alpha}$, the cost of deceased individuals $c_{D,\alpha}$, and the impact on epidemic-related loss of economic labor force $c_{L,\alpha}$. Following Gros et al. (2021), the proportionality factors of cost can be expressed in relation to annual GDP per capita (for OECD countries), allocating a cost of 0.140 on the infected fraction when the value of life cost is omitted. In the SEIRSD model, this cost is re-scaled to the death component by applying the ratio of the mean transition periods (I to R flow and I to D flow), i.e., δ_2/ν.

The population-specific implementation cost of their control strategy, $c_{\text{cs},\alpha} \in \mathbb{R}$, $\alpha \in \{0, 1\}$ and cs $\in CS$, is separated along confinement, vaccination and isolation type and summed when strategies are combined:

$$c_{\text{cs},\alpha} \in [0, c_{\text{Css}}, c_{\text{Cwl}}, c_{\text{Vel}}, c_{\text{Vlh}}, c_{\text{Css}}+c_{\text{Vel}}, c_{\text{Css}}+c_{\text{Vlh}}, c_{\text{Cwl}}+c_{\text{Vel}}, c_{\text{Cwl}}+c_{\text{Vlh}}]_{\alpha} \quad \text{(C.3)}$$

incremented with $c_{\text{Ifs}_{01}}$ or $c_{\text{Ipl}_{01}}$ for effective isolation strategies. The direct summation of cost summands assumes no interference nor synergy with respect to the total cost of hybrid strategies. The simulation is implemented for two subpopulations with a GDP difference factor $(1\text{-}\,\text{GDP}_{\text{diff}})$, with $\text{GDP}_{\text{diff}} = .1$. Subpopulation 1 is the reference, and subpopulation group-0 is corrected for its limited resources by a factor $(1\text{-}\,\text{GDP}_{\text{diff}})$.

The cost of intervention from the implemented control strategy, $c_{\text{cs},\alpha}$, is scaled in relation to health policy deployment, cost of life, and loss of productivity by a factor CS_{scale}. To assess the impact of the relative size of this intervention cost on the choice of the optimal control strategy, a variable range of CS_{scale} has been tested, $CS_{\text{scale}} = 1.5$.[8] The relative cost CV_{ratio} of deploying a confinement strategy versus a vaccination strategy is also variable. We estimate the relative deployment cost of confinement, based on the analysis of Gollier (2021) on the cost of vaccination, to range in smaller fractions of the latter; $CV_{\text{ratio}} = .1$, resulting in respective cost scale factors for confinement, $C_{\text{scale}} = CV_{\text{ratio}} CS_{\text{scale}}$, and vaccination, $V_{\text{scale}} = CS_{\text{scale}}$. The cost correlation factors are implemented as follows:

$$c_I = c_L = 0.140 \cdot [1\text{-}\,\text{GDP}_{\text{diff}}, 1], \quad c_D = 0.155\, \delta_2/\nu \cdot [1\text{-}\,\text{GDP}_{\text{diff}}, 1], \quad \text{(C.4)}$$

where the GDP-differentiated correlation factors $c_{I,\alpha}$, $c_{D,\alpha}$, and $c_{L,\alpha}$ for the two populations α are juxtaposed in the list; e.g., $c_I = [c_{I,0}, c_{I,1}]$. The parameters of the confinement strategy impact its operation cost. The relative confinement duration and the relative severity of contact reduction are implemented as proportional factors, with a lower operation cost in the country with the relatively lower GDP. Formally, the confinement severity is expressed as a relative deviation from the average number of contacts

[8] In (Broekaert et al., 2024c) a more extensive range $CS_{\text{scale}} \in \{.4, 1, 1.5, 2, 3, 4, 5\}$ and $CV_{\text{ratio}} \in \{.1, .2\}$ and $\text{GDP}_{\text{diff}} \in \{.05, .1, .15, .20\}$ is reported and tested.

under normal circumstances without an epidemic:

$$c_{\text{Css}} = \text{scaleC} \cdot \left(\frac{D_T - D_S}{D_T} \right) \cdot \frac{\text{dur}_{\text{Css}}}{\text{dur}_{\text{Cwl}}} \left[(1 - \text{GDP}_{\text{diff}}), 1 \right], \tag{C.5}$$

$$c_{\text{Cwl}} = \text{scaleC} \cdot \frac{D_T - D_W}{D_T} \cdot \frac{\text{dur}_{\text{Cwl}}}{\text{dur}_{\text{Cwl}}} \cdot \left[(1 - \text{GDP}_{\text{diff}}), 1 \right]. \tag{C.6}$$

While for isolation types the cost is estimated similarly

$$c_{\text{Ifs}_{01}} = \frac{\text{dur}_{\text{Ifs}}}{\text{dur}_{\text{Ipl}}} \left[(1 - \text{GDP}_{\text{diff}}), 1 \right], \tag{C.7}$$

$$c_{\text{Ipl}_{01}} = \frac{\text{dur}_{\text{Ipl}}}{\text{dur}_{\text{Ipl}}} \cdot (\text{frac\_isol}^2) \left[(1 - \text{GDP}_{\text{diff}}), 1 \right], \tag{C.8}$$

where a non-linear dependence is assumed in the severity of closing of the frontiers.

The operation and development cost of the vaccination strategy is expressed by the factors of i) vaccine efficacy (e), reflecting advanced pharmaceutical technology, ii) relative duration of the industrial development and deployment process and, iii) presumed higher required investment costs in the lower-GDP country.

$$c_{\text{Vel}} = V_{\text{scale}} e_{\text{Vel}} \left(\frac{t_{\text{start}_{\text{Vel}}}}{t_{\text{start}_{\text{Vlh}}}} \right) \cdot [1 + \text{GDP}_{\text{diff}}, 1], \tag{C.9}$$

$$c_{\text{Vlh}} = V_{\text{scale}} e_{\text{Vlh}} \left(\frac{t_{\text{start}_{\text{Vlh}}}}{t_{\text{start}_{\text{Vlh}}}} \right) \cdot [1 + \text{GDP}_{\text{diff}}, 1], \tag{C.10}$$

Appendix D. Game matrices for ECC

The multiple ECC-based Nash strategy profiles for the isolation types Igo_{01}, Ifs_{01}, and Ipl_{01} need to be compared and one selected.

Igo$_{01}$	No$_1$	Css$_1$	Cwl$_1$	Vel$_1$	Vlh$_1$	CssVel$_1$	CssVlh$_1$	CwlVel$_1$	CwlVlh$_1$
No$_0$	0.252 0.227	0.248 0.249	0.236 0.226	0.214 0.226	0.376 0.227	0.205 0.225	0.357 0.226	0.213 0.225	0.368 0.226
Css$_0$	0.250 0.252	0.246 0.252	0.234 0.252	0.212 0.251	0.375 0.252	0.204 0.251	0.356 0.252	0.211 0.251	0.366 0.252
Cwl$_0$	0.250 0.257	0.246 0.256	0.234 0.257	0.213 0.256	0.375 0.257	0.204 0.256	0.356 0.256	0.212 0.256	0.366 0.257
Vel$_0$	0.250 0.241	0.245 0.240	0.233 0.240	0.211 0.239	0.373 0.240	0.203 0.239	0.354 0.240	0.210 0.239	0.365 0.240
Vlh$_0$	0.251 0.389	0.247 0.388	0.236 0.388	0.213 0.388	0.376 0.388	0.205 0.387	0.357 0.388	0.213 0.387	0.368 0.388
CssVel$_0$	0.248 0.246	0.243 0.245	0.231 0.245	0.210 0.245	0.372 0.245	0.202 0.244	0.327 0.245	0.210 0.244	0.364 0.245
CssVlh$_0$	0.250 0.392	0.246 0.391	0.234 0.392	0.212 0.391	0.374 0.392	0.204 0.391	0.330 0.391	0.211 0.391	0.366 0.391
CwlVel$_0$	0.249 0.227	0.244 0.249	0.232 0.226	0.211 0.225	0.373 0.226	0.202 0.225	0.327 0.226	0.210 0.225	0.364 0.226
CwlVlh$_0$	0.250 0.397	0.246 0.396	0.234 0.396	0.212 0.396	0.375 0.397	0.204 0.395	0.330 0.396	0.212 0.395	0.366 0.396

Ifs$_{01}$	No$_1$	Css$_1$	Cwl$_1$	Vel$_1$	Vlh$_1$	CssVel$_1$	CssVlh$_1$	CwlVel$_1$	CwlVlh$_1$
No$_0$	0.314 0.286	0.305 0.309	0.292 0.286	0.273 0.286	0.435 0.286	0.265 0.309	0.387 0.286	0.246 0.286	0.424 0.286
Css$_0$	0.340 0.311	0.305 0.312	0.292 0.311	0.273 0.311	0.435 0.311	0.266 0.312	0.387 0.311	0.272 0.311	0.424 0.311
Cwl$_0$	0.314 0.316	0.305 0.316	0.292 0.292	0.273 0.316	0.435 0.292	0.265 0.316	0.387 0.292	0.246 0.292	0.398 0.292
Vel$_0$	0.314 0.300	0.304 0.300	0.291 0.300	0.273 0.300	0.435 0.300	0.265 0.300	0.387 0.300	0.246 0.300	0.423 0.300
Vlh$_0$	0.314 0.447	0.305 0.447	0.292 0.447	0.273 0.447	0.435 0.447	0.265 0.447	0.387 0.447	0.246 0.447	0.398 0.447
CssVel$_0$	0.314 0.305	0.305 0.306	0.292 0.305	0.273 0.305	0.435 0.282	0.265 0.305	0.387 0.282	0.246 0.282	0.423 0.282
CssVlh$_0$	0.314 0.451	0.305 0.451	0.292 0.451	0.273 0.451	0.435 0.451	0.265 0.451	0.387 0.451	0.246 0.451	0.398 0.451
CwlVel$_0$	0.314 0.286	0.304 0.309	0.291 0.286	0.273 0.286	0.435 0.286	0.265 0.286	0.387 0.286	0.246 0.286	0.397 0.286
CwlVlh$_0$	0.314 0.455	0.304 0.455	0.292 0.455	0.273 0.455	0.435 0.455	0.265 0.455	0.387 0.455	0.246 0.455	0.398 0.455

Ipl$_{01}$	No$_1$	Css$_1$	Cwl$_1$	Vel$_1$	Vlh$_1$	CssVel$_1$	CssVlh$_1$	CwlVel$_1$	CwlVlh$_1$
No$_0$	0.320 0.288	0.316 0.311	0.305 0.288	0.282 0.287	0.445 0.288	0.273 0.287	0.426 0.288	0.282 0.287	0.437 0.288
Css$_0$	0.319 0.314	0.314 0.313	0.302 0.313	0.281 0.313	0.443 0.314	0.273 0.312	0.424 0.313	0.280 0.312	0.435 0.313
Cwl$_0$	0.319 0.319	0.315 0.318	0.303 0.318	0.281 0.318	0.444 0.319	0.273 0.317	0.424 0.318	0.281 0.318	0.435 0.318
Vel$_0$	0.318 0.302	0.313 0.302	0.301 0.302	0.280 0.301	0.442 0.302	0.271 0.301	0.422 0.302	0.279 0.301	0.433 0.302
Vlh$_0$	0.320 0.450	0.316 0.449	0.304 0.450	0.282 0.449	0.444 0.450	0.273 0.449	0.425 0.449	0.281 0.449	0.436 0.450
CssVel$_0$	0.317 0.307	0.312 0.307	0.300 0.307	0.279 0.306	0.441 0.307	0.271 0.306	0.396 0.307	0.278 0.306	0.432 0.307
CssVlh$_0$	0.318 0.454	0.314 0.453	0.302 0.453	0.281 0.453	0.443 0.454	0.272 0.452	0.398 0.453	0.280 0.452	0.434 0.453
CwlVel$_0$	0.317 0.288	0.312 0.311	0.300 0.288	0.279 0.287	0.441 0.288	0.271 0.287	0.396 0.287	0.278 0.287	0.432 0.288
CwlVlh$_0$	0.319 0.459	0.315 0.458	0.302 0.458	0.281 0.457	0.443 0.459	0.273 0.457	0.398 0.458	0.280 0.457	0.435 0.458

Table D.5: The ECC pay-off matrices for the first Wave, Isolation type: Igo_{01} (top), Ifs_{01} (middle), Ipl_{01} (bottom), and $\text{GDP}_{\text{diff}} = 0.15$; $CS_{\text{scale}} = 1.5$ and $CV_{\text{ratio}} = .1$ with selected Nash equilibrium for the **Cwl**$_0$**_Vel**$_0$**_Css**$_1$**_Vel**$_1{}^\star$ control configuration, as appears in Table 3.